CHEMISTRY
A European Journal

Supporting Information

Electronic Modifications of Fluorescent Cytidine Analogues Control Photophysics and Fluorescent Responses to Base Stacking and Pairing

Kristine L. Teppang[+], Raymond W. Lee[+], Dillon D. Burns[+], M. Benjamin Turner, Melissa E. Lokensgard, Andrew L. Cooksy, and Byron W. Purse*[a]

chem_201803653_sm_miscellaneous_information.pdf

Table of Contents

1. Supplemental Figures

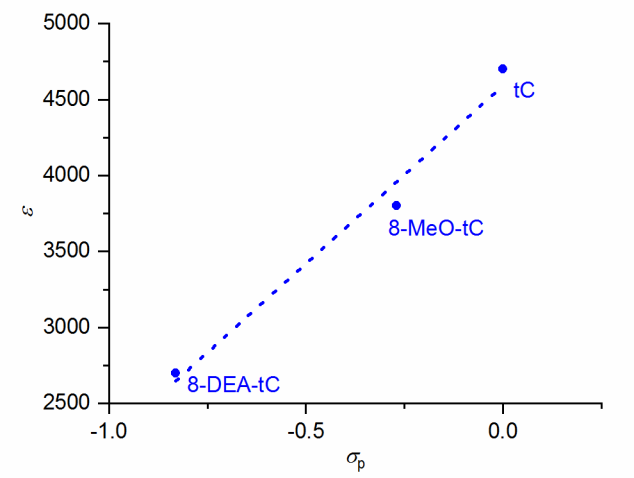

Figure S1. Extinction coefficients ε for the tC compounds are linearly correlated with Hammett σ_p.

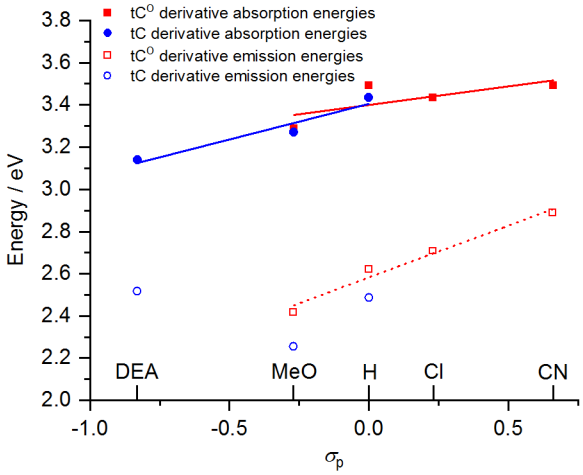

Figure S2. Correlation of the absorption and fluorescence emission energies, each at λ_{max}, of tC^O compounds (red) and tC compounds (blue) with Hammett σ_p for each substituent (listed above the *x*-axis).

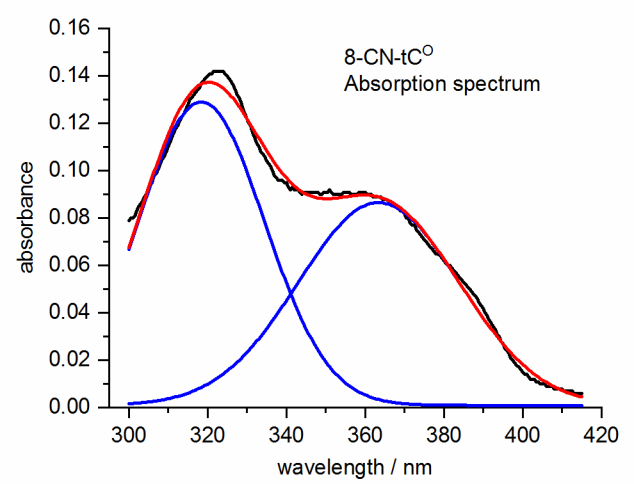

Figure S3. Fitting the 8-CN-tC^{O} absorption spectrum to two Gaussian curves shows (blue; sum of Gaussian curves in red) shows that, at 355 nm, 89% of the absorption comes from the longer wavelength absorption.

2. General Experimental Section

All reagents and chemicals used were purchased from Acros Organics and Fisher Chemical at ACS grade or higher quality and used as received without further purification, except as noted. 5-Amino-2-methylbenzothiazole was obtained from Alfa Aesar and 2-cyanoethyl-*N*,*N*,*N*′,*N*’-tetraisopropylphosphorodiamidite was obtained from Sigma-Aldrich. The synthesis of nucleoside precursors 8-Cl-tC^{O} and 8-MeO-tC for tritylation and phosphoramidite synthesis has been previously described.[1] Solvents used for UV/vis and fluorescence measurements were spectrophotometric grade or were aqueous buffers prepared using Milli-Q water.

NMR (^{1}H and ^{13}C) spectra were acquired on Varian 400 MHz, Varian 500 MHz, and Buker 600 MHz NMR spectrometers and recorded at 298 K. Chemical shifts are referenced to the residual solvent peaks and given in parts per million (ppm). Splitting patterns are denoted as s (singlet), d (doublet), dd (doublet of doublet), t (triplet), q (quartet), and m (multiplet). Fluorescence measurements were recorded on a PTI Quantamaster QM-400 fluorescence spectrophotometer and corrected using the manufacturer’s calibration files. Absorbance measurements were taken on a Shimadzu Pharma Spec 1700 UV-Vis spectrophotometer. CD spectroscopy was performed on an Aviv Model 420 and recorded at 298 K. High-resolution electrospray ionization (ESI) mass spectrometry was performed at the University of California Riverside High Resolution Mass Spectrometry Facility using an Agilent LC-TOF in ESI mode.

Synthetic steps that required an inert atmosphere were carried out under dried nitrogen gas using standard Schlenk techniques.

3. Computational Methods

Ground state geometries were optimized by density functional theory (DFT), and excited state geometries and energies obtained by time-dependent DFT (TDDFT). A small series of benchmark calculations was carried out on parent tC^O using every combination of B3LYP,[2,3] BH&HLYP,[3,4] PBE0,[5] and M06[6] methods with SVP,[7] TZVP,[8] cc-pVDZ,[9] and pc-2[10] basis sets. Solvation was modeled by optimizing the geometry with explicit water molecules hydrogen-bonding to the carbonyl oxygen and to the S or O atom at the center of the tricyclic system, and then applying the IEFPCM continuum solvation model[11] to the entire system. For the B3LYP method, Grimme's D2 empirical dispersion model[12] was applied as well. The best agreement with experimental excitation and emission spectra was found for B3LYP-D2/cc-pVDZ and this methodology was applied to the remaining calculations described in this paper. All calculations were carried out using Gaussian 09;[13] some basis sets were transcribed from the EMSL Basis Set Exchange.[14]

Table S1. Summary results from B3LYP/cc-pVDZ+D2 optimizations: number of contracted basis functions, energy, and free energy (298.15K) at the optimized geometries.

species	# functions	energy	free energy
		(Eh)	(Eh)
8-CN-tCo	292	-831.62569	-831.48014
8-Cl-tCo	282	-1198.99	-1198.8544
tCo	269	-739.37499	-739.22553
8-OCH3-tCo	307	-853.90741	-853.72953
tC	273	-1062.3675	-1062.2205
8-OCH3-tC	311	-1176.9012	-1176.7254
8-DEA-tC	340	-1196.3523	-1196.1386

Table S2. Predicted absorption λ_{max} values (bold, nm), absorbance values, and Stokes shifts (italic, nm) for tC^O at selected DFT methods and basis sets. The experimental values are λ_{max}=355 nm, A = 8000, Stokes shift = 118 nm. Solvation was modeled optimizing with two explicit H_2O molecules and including an IEFPCM solvation model for water.

	cc-pVDZ	SVP	TZVP	pc-2
B3LYP	**348** 7000 *85*	**348** 7000 *82*	**344** 6600 *93*	**348** 7500 *76*

BHHLYP	**293** 10000 *74*	**293** 10000 *74*	**295** 10000 *77*	**295** 10300 *67*
M06	**338** 7500 *82*	**338** 7300 *71*	**340** 7600 *77*	**340** 7800 *73*
PBE0	**338** 7300 *84*	**335** 7300 *80*	**338** 7800 *82*	**338** 8000 *74*

The data for Table 4 in the paper were obtained from calculations on duplexes of the trimers of form WXY, where X=8-DEA-tC, W=C or G, Y=A or C. The B3LYP DFT method was used, with a cc-pVDZ basis for the tC subunit and 3-21G for the remainder of the complex. The HOMO and LUMO for the tC subunit were determined by visual inspection of the MOs. (In general there are higher energy occupied MOs and lower energy unoccupied MOs with density localized to other bases, and believed not to be relevant to the fluorescence signal). Orbital coefficients at each atom were squared and summed to obtain the total density over each subunit of the complex. Table S3 summarizes the energies and the electron densities one each of the three bases in the WXY trimer.

Table S3. B3LYP/cc-pVDZ(tC^{O}),3-21G calculated 8-DEA-tC HOMO and LUMO energies and total electron densities on components of selected duplex trimers based on WXY where X=8-DEA-tC, W=C or G, Y=A or C. Electron densities given are relative to the total density on the entire duplex trimer including deoxyribose-phosphate backbones, so totals are less than one.

	HOMO					**LUMO**				
WXY	**MO#**	**E (Eh)**	**W**	**X**	**Y**	**MO#**	**E (Eh)**	**W**	**X**	**Y**
CXA	494	-0.23478	0.0013	0.4063	0.0032	496	-0.22244	0.0005	0.2261	0.0102
GXA	495	-0.23024	0.0853	0.1872	0.0127	497	-0.21819	0.1677	0.3706	0.0399
GXC	492	-0.23628	0.2316	0.3729	0.0008	497	-0.21942	0.1722	0.3196	0.0008

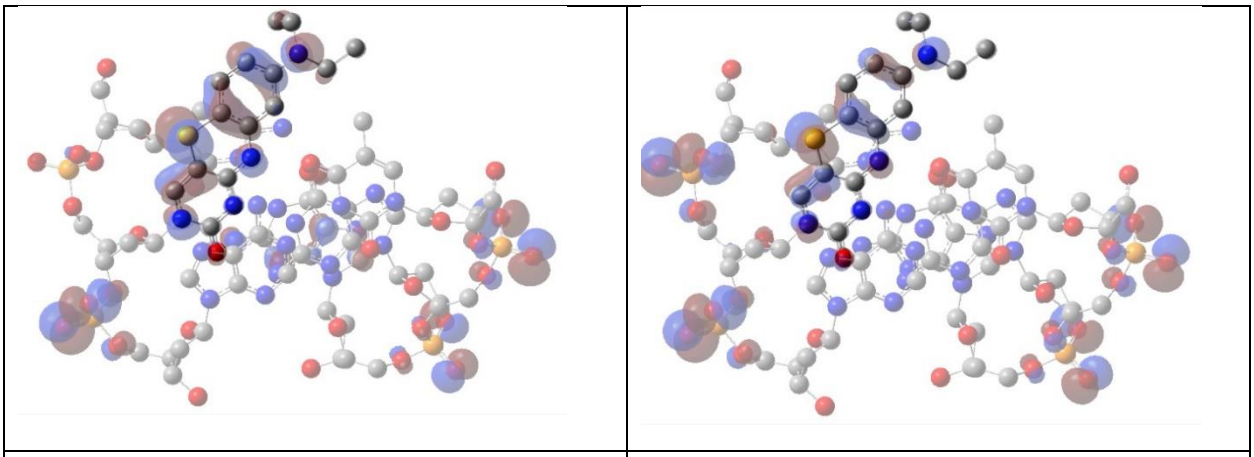

(a) CXA HOMO

(b) CXA LUMO

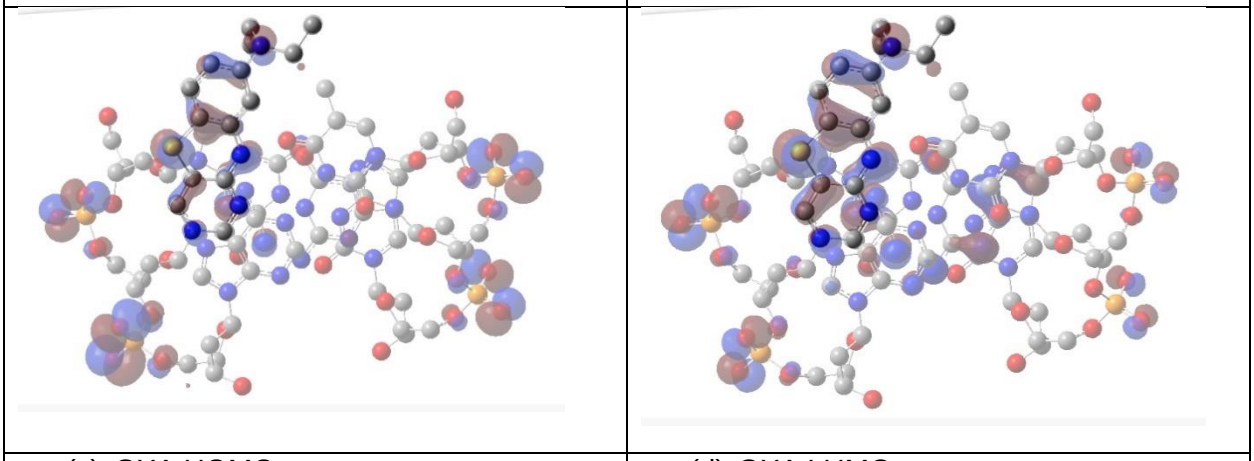

(c) GXA HOMO

(d) GXA LUMO

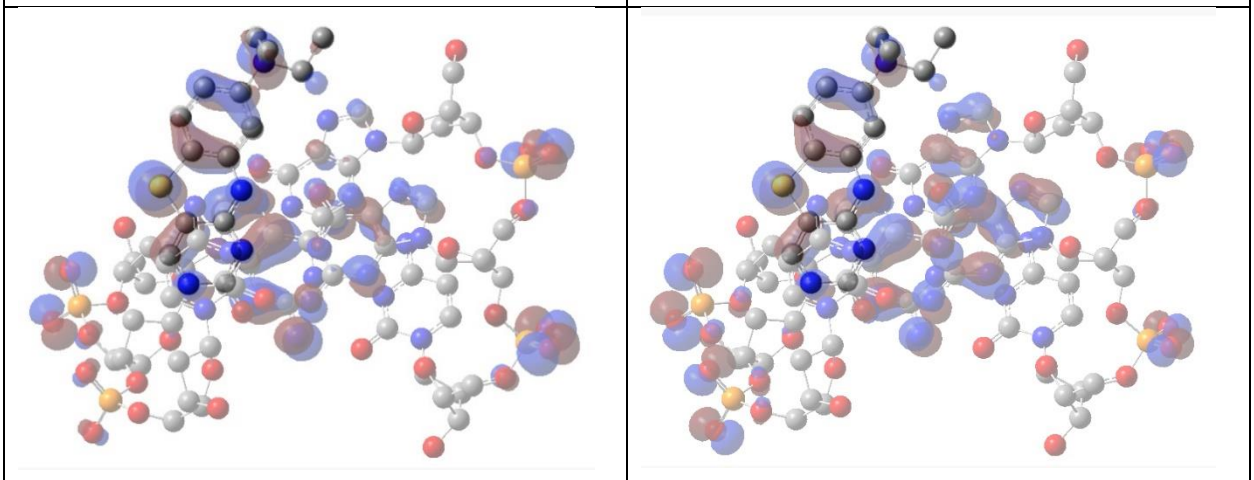

(e) GXC HOMO

(f) GXC LUMO

Table S4. Molecular orbital isosurfaces for the 8-DEA-tC HOMO and LUMO in selected duplex trimers (X=8-DEA-tC). H atoms have been deleted for clarity, and the 8-DEA-tC subunit has been highlighted. The increased delocalization of the orbitals when complexed to G is visible particularly in (d)—(f).

3. Synthetic Details

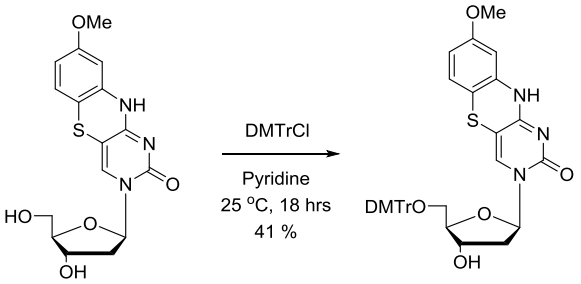

8-Methoxy-tC 2'-deoxy-5'-*O*-(4,4-dimethoxytrityl)-β-D-ribonucleoside

8-Methoxy-tC 2'-deoxy-*β*-D-ribonucleoside (156 mg, 0.429 mmol) was placed in a clean dry 25-mL side-armed round-bottomed flask. To this was added 3 mL of anhydrous pyridine under N_2 and the reaction mixture was stirred at room temperature for 5 minutes. Dimethoxytritylchloride (290 mg, 0.860 mmol) was added and the reaction was stirred at room temperature for 18 hours. The reaction was monitored by TLC (10% MeOH in CH_2Cl_2). The reaction was quenched with MeOH and the solvent was evaporated by rotary evaporation. The crude product was purified by flash chromatography (10% MeOH in CH_2Cl_2 with 1% triethylamine). The product was isolated as a yellow solid (118 mg, 41 %). **^{1}H NMR (400 MHz, $CDCl_3$)**: δ 9.45 (bs, 1H), 7.67 (s, 1H), 7.43 (m, 2H), 7.31 (m, 6H), 7.23 (t, J=7.16, 1H), 6.83 (m, 4H), 6.80 (d, J=2.6 Hz, 1H), 6.65 (d, J=8.6 Hz, 1H), 6.41 (dd, J=8.6, 2.5 Hz, 1H), 6.37 (t, J=6.4 Hz, 1H), 4.52 (m, 1H), 4.15 (m, 1H), 3.75 (s, 3H), 3.74 (s, 3H), 3.72 (s, 3H), 3.35 (m, 2H), 2.81 (m, 1H), 2.21 (m, 1H).

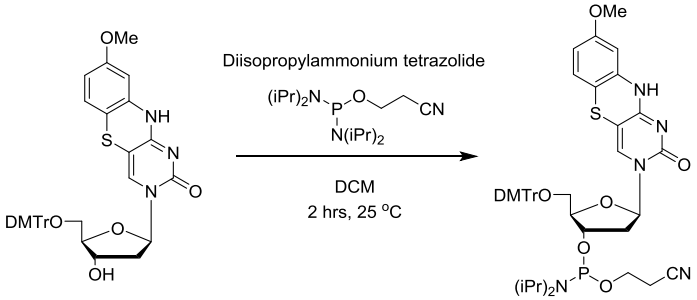

8-Methoxy-tC 2'-deoxy-5'-*O*-(4,4-dimethoxytrityl)-3'-O-[2-cyanoethoxy-(N,N-diisopropylamino)phosphino]-β-D-deoxyribonucleoside

8-Methoxy-tC 2'-deoxy-5'-*O*-(4,4-dimethoxytrityl)-β-D-ribonucleoside (118 mg, 0.177 mmol) was placed in a clean dry 25-mL Schlenk tube. To this was added 3 mL of anhydrous DCM under N_2. Diisopropylammonium tetrazolide (122 mg, 7.10 mmol) was then added to the reaction mixture. The reaction mixture was thoroughly degassed and to this was added 2-cyanoethyl *N*,*N*,*N'*,*N'*-tetraisopropyl phosphoramidite (113 µL, 0.354 mmol) and the reaction was stirred at room temperature. The reaction was monitored by TLC (10% EtOAc in hexanes) and found to be complete after 2 hours. The solvent was evaporated to dryness and the product was purified via flash chromatography. (MeOH in DCM with 1% triethylamine). **^{1}H NMR (400 MHz, $CDCl_3$)** δ 9.55 (bs, 1H), 7.32 (m, 9H), 6.95 (m, 1H), 6.85 (m, 4H), 6.68 (t, J=6.5 Hz, 1H), 6.47 (m, 1H), 6.23 (m, 1H), 4.60 (m, 1H), 4.19 (m, 1H), 3.78 (s, 9H), 3.57 (m, 3H), 3.42 (m, 3H), 2.60 (t, J=6.33 Hz, 2H), 2.42 (m, 2H), 2.24 (m, 1H), 1.26 (m, 9H), 1.16 (m, 3H). **^{31}P NMR (162 MHz,**

$CDCl_3$) δ 149.16, 148.41. HRMS (ESI) calcd. for $C_{46}H_{52}N_5O_8PS$ 865.3274, found 864.3158 [M-H]$^-$.

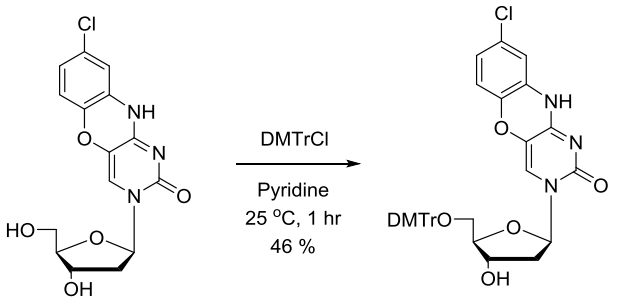

8-Chloro-tC^O 2'-deoxy-5'-*O*-(4,4-dimethoxytrityl)-β-D-ribonucleoside

8-Chloro-tC 2'-deoxy-*β*-D-ribonucleoside (107 mg, 0.304 mmol) was placed in a dry 25-mL Schlenk tube and dissolved in 5 mL of pyridine. Then, 4, 4-dimethoxytrityl chloride (206 mg, 0.608 mmol) was added at room temperature. The reaction was monitored by TLC (10% MeOH in CH_2Cl_2) and found to be complete at 1 hour. The reaction was quenched by adding excess methanol. The solvent was evaporated from the crude which was then purified using flash chromatography (0 → 10% MeOH in CH_2Cl_2). The product was isolated as a yellow solid (91.5 mg, 46 %). **^{1}H NMR ($CDCl_3$, 400 MHz)** δ 10.2 (bs, 1H), 7.49-7.38 (m, 10H), 7.43 (d, 1H), 6.84 (m, 4H), 6.70 (m, 1H), 6.34 (m, 2H), 4.55 (m, 1H), 4.07 (m, 1H), 3.77 (s, 3H), 3.75 (s, 3H), 3.38 (m, 2H), 2.65 (m, 1H), 2.28 (m, 1H).

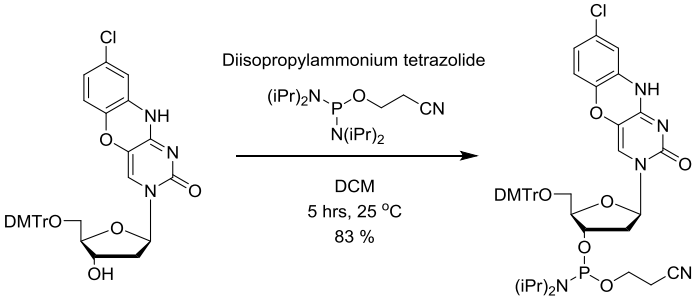

8-Chloro-tC^O 2'-deoxy-5'-*O*-(4,4-dimethoxytrityl)-3'-O-[2-cyanoethoxy-(N,N-diisopropylamino)phosphino]-β-D-deoxyribonucleoside

Diisopropylammonium tetrazolide (32 mg, 0.19 mmol) was added to a small round-bottom flask under N_2. The flask was placed in an ice bath (2 °C), and 2-cyanoethyl *N*,*N*,*N'*,*N'*-tetraisopropyl phosphoramidite (60 µL, 0.19 mmol) was slowly added. The mixture was allowed to warm to room temperature before adding 2 mL dry DCM. During this time, 8-chloro-tC^O 2'-deoxy-5'-*O*-(4,4-dimethoxytrityl)-β-D-ribonucleoside (92.6 mg, 0.141 mmol) was placed in a dry 25-mL Schlenk tube under N_2 and dissolved in 1 mL DCM. The phosphoramidite solution was transferred to the flask containing the protected nucleoside and the reaction stirred for 5 hours at room temperature under nitrogen. The crude was purified via flash chromatography (90% ethyl acetate in hexanes with 1% triethylamine). The product was isolated as a yellow solid (99.7 mg, 83 %). **^{1}H NMR (400 MHz, $CDCl_3$)** δ 9.56 (bs, 1H), 7.48-7.32 (m, 11H), 7.21 (m, 1H), 6.82 (m, 4H), 6.74 (m, 1H), 6.34 (m, 1H), 6.26 (m, 1H), 4.62 (m, 1H), 4.13 (m, 1H), 3.77 (s, 3H), 3.75 (s, 3H), 3.64-3.48 (m, 4H), 3.36 (m, 1H), 2.62 (t, J=6.3 Hz, 2H), 2.45 (t, J=6.4 Hz, 1H), 2.25

(m, 1H), 1.18 (d, J=6.8 Hz, 9H), 1.09 (m, 3H). **^{31}P NMR (162 MHz, $CDCl_3$)** δ 149.00, 148.54. HRMS (ESI) for $C_{45}H_{49}ClN_5O_8P$ calc. 853.3007, found 852.2929 $[M-H]^-$.

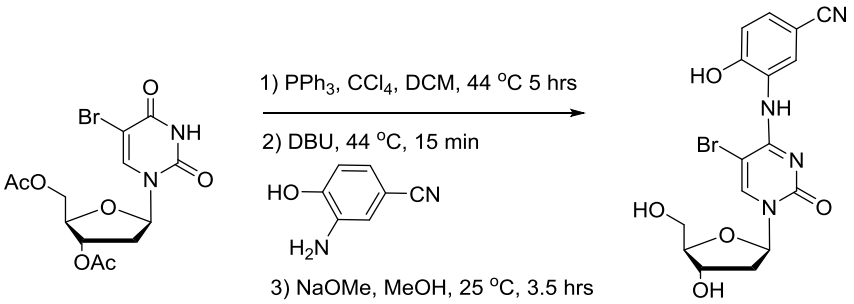

5-Bromo-N4-(2-hydroxy-5-cyanophenyl)-2'-deoxycytidine

Carbon tetrachloride dried over 4 Å molecular sieves (4.3 mL) was combined with dry DCM (5 mL) under N_2 and was stirred at room temperature 10 minutes. Triphenylphosphine (639 mg, 2.44 mmol) was added and the reaction was continued at room temperature for 15 minutes. 3',5'-Diacetyl-5-bromo-2'-deoxyuridine (500 mg, 1.28 mmol) was added to the reaction and it was heated at 44 °C. After 5 hours, a premixed solution of 4-cyano-2-aminophenol (172 mg, 1.28 mmol) with DBU (190 µL, 1.28 mmol) was added to 1 mL of dry DCM and the reaction and stirred at 44 °C for 15 minutes. The reaction was evaporated and purified by flash chromatography (MeOH in DCM, 0-5 %) to yield the protected secondary amine as a semi-crude product mixture. This mixture was combined from multiple reactions, dissolved in methanol (10-100 mg/mL) under N_2 and sodium methoxide 30% in methanol (922 µL, 5.12 mmol) was added and the reaction stirred at room temperature for 3.5 hours. Acetic acid was added to quench the reaction and the solvent was removed by rotary evaporation. **^{1}H NMR (400 MHz, $(CD_3)_2SO$)** δ 8.51 (d, J=2.4Hz, 1H), 8.34 (s, 1H), 6.97 (dd, J= 8.5, 2.4 Hz, 1H), 6.19 (d, J=8.5 Hz, 1H), 6.13 (t, J=6.4 Hz, 1H), 4.24 (m, 1H), 3.80 (q, J=3.4 Hz, 1H), 3.61 (m, 2H), 2.19 (m, 1H), 2.07 (m, 1H).

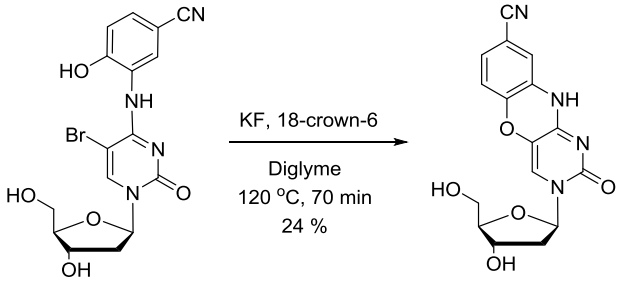

8-Cyano-tC^O 2'-deoxy-β-D-ribonucleoside

5-Bromo-N-4-(2-hydroxy-5-cyanophenyl)-2'-deoxycytidine (500 mg, 1.18 mmol) was dissolved in dry diglyme (4 mL) with 18-crown-6 (3.12 g, 11.8 mmol) under N_2, then potassium fluoride (462 mg, 11.8 mmol) was added. The reaction was heated to 120°C and stirred for 70 minutes, cooled to room temperature, and purified flash chromatography using Redisep Gold High Performance diol columns (MeOH in DCM, 0-10%) to yield the product (90 mg, 24%). **^{1}H NMR (MeOD)** δ 8.56 (bs, 1H), 7.77 (s, 1H), 7.25 (dd, J=8.3, 1.6 Hz, 1H), 7.06 (s, 1H), 6.89 (d, J=8.6 Hz, 1H), 6.22 δ 7.48 (s, 1H), 6.83 (dd, J=8.5, 2.5 Hz, 1H), 6.80-6.68 (m, 2H), 6.12 (dd, J=7.3, 6.0 Hz, 1H), 4.24 (dt, J=6.3, 3.3 Hz, 1H), 3.76 (q, J=3.3 Hz, 1H), 3.58 (t, J=3.6 Hz, 2H), 2.10-

1.98 (m, 2H). **^{13}C NMR (600 MHz, $(CD_3)_2SO$)** δ 173.28, 166.11, 155.48, 153.64, 140.79, 129.74, 123.23, 119.52, 115.79, 88.40, 87.50, 85.60, 69.85, 60.81, 40.79, 23.35. HRMS (ESI) calcd. for $C_{16}H_{16}N_4O_5$ 342.0964, found 341.0895 $[M-H]^-$.

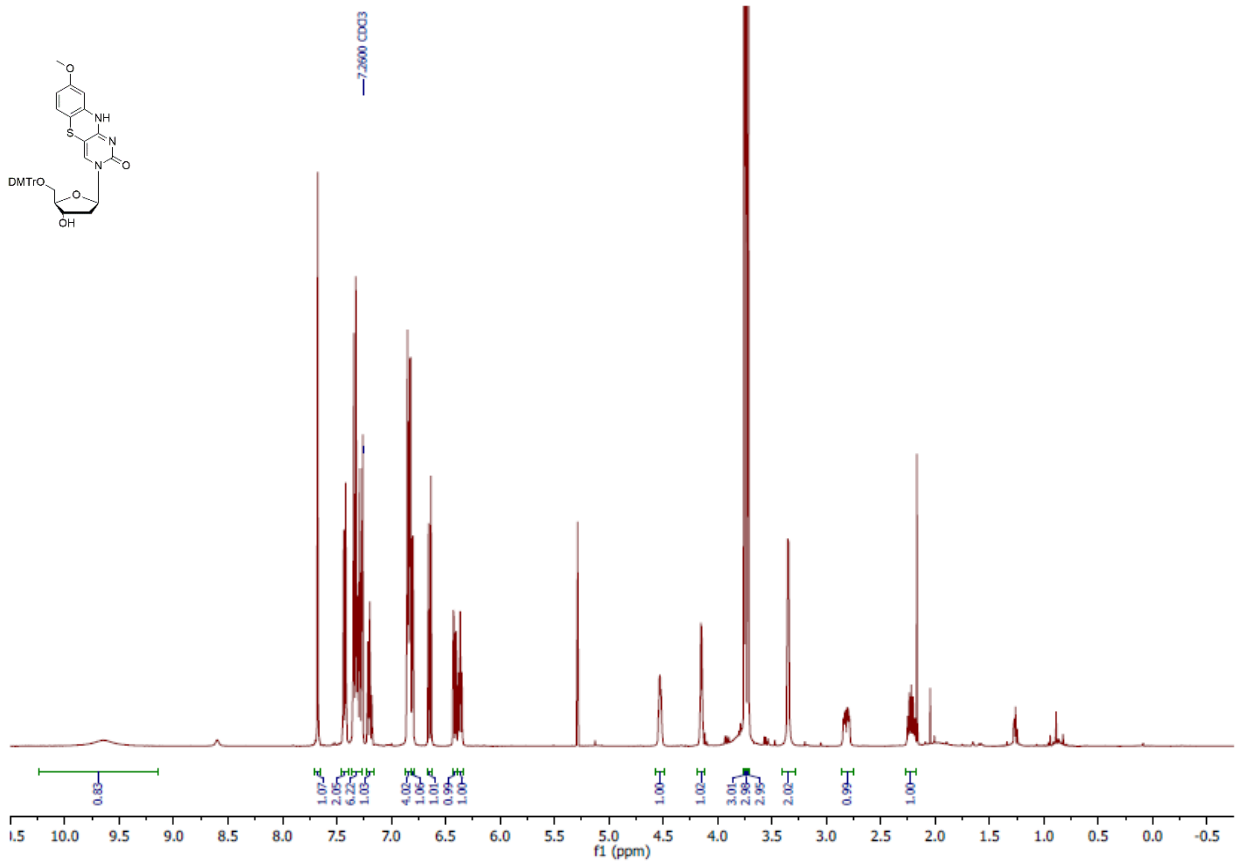

Figure S3. ^{1}H NMR of 8-methoxy-tC 2'-deoxy-5'-*O*-(4,4-dimethoxytrityl)-β-D-ribonucleoside. Spectrum acquired at 298 K, $CDCl_3$, 400 MHz.

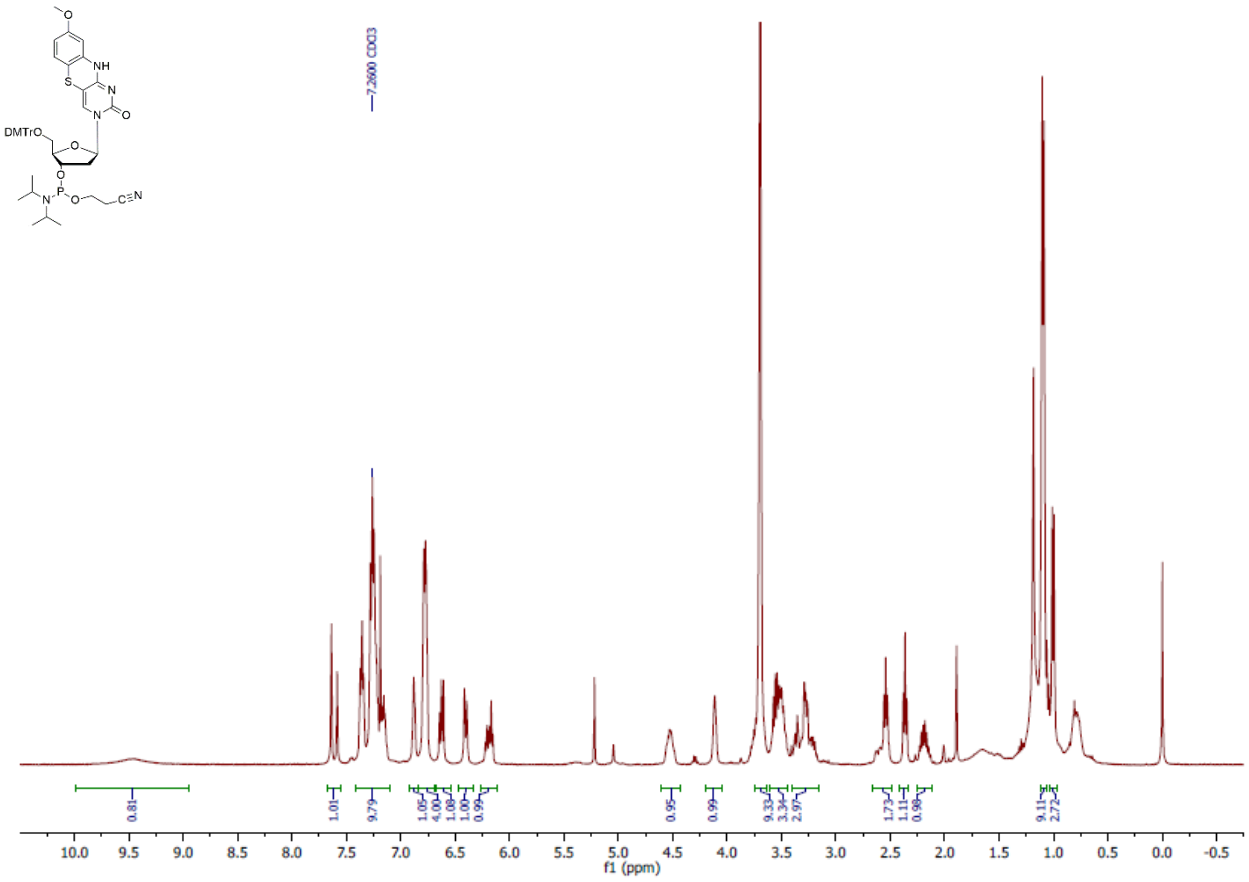

Figure S4. ^{1}H NMR of 8-Methoxy-tC 2'-deoxy-5'-*O*-(4,4-dimethoxytrityl)-3'-O-[2-cyanoethoxy-(N,N-diisopropylamino)phosphino]-β-D-ribonucleoside. Spectrum acquired at 298 K, $CDCl_3$, 400 MHz.

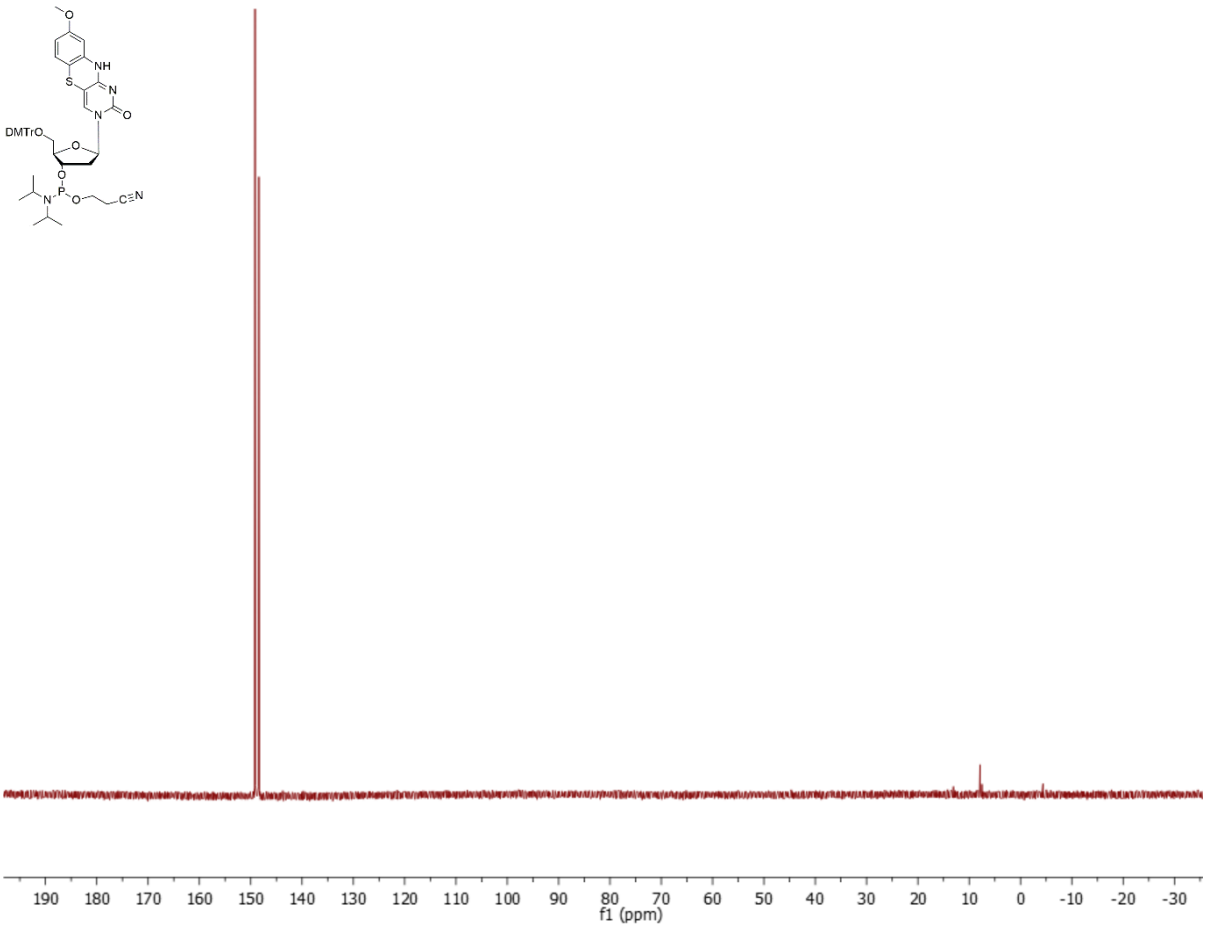

Figure S5. ^{31}P NMR of 8-Methoxy-tC 2'-deoxy-5'-*O*-(4,4-dimethoxytrityl)-3'-O-[2-cyanoethoxy-(N,N-diisopropylamino)phosphino]-β-D-ribonucleoside. Spectrum acquired at 298 K, $CDCl_3$, 162 MHz.

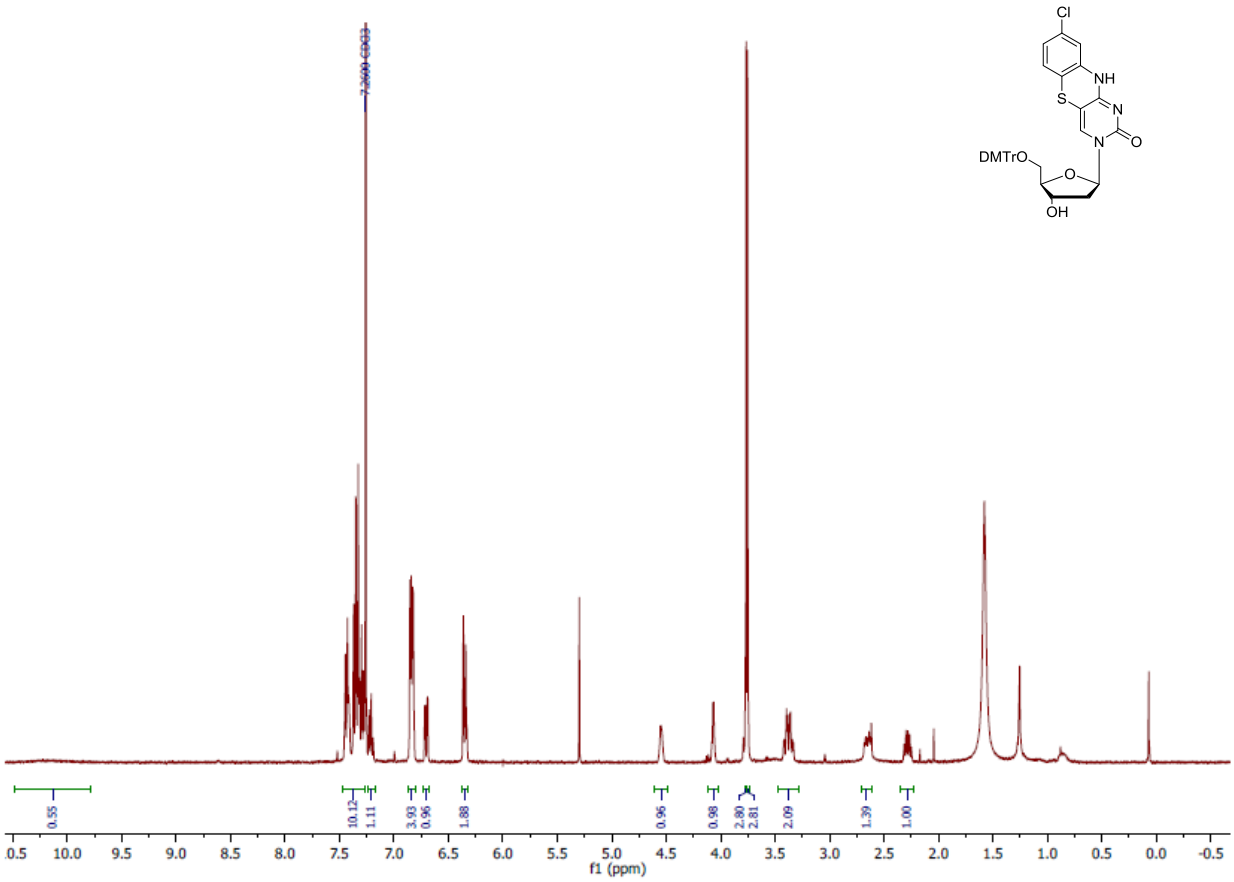

Figure S6. ^{1}H NMR of 8-Chloro-tC^{O} 2'-deoxy-5'-*O*-(4,4-dimethoxytrityl)-β-D-ribonucleoside. Spectrum acquired at 298 K, $CDCl_3$, 400 MHz.

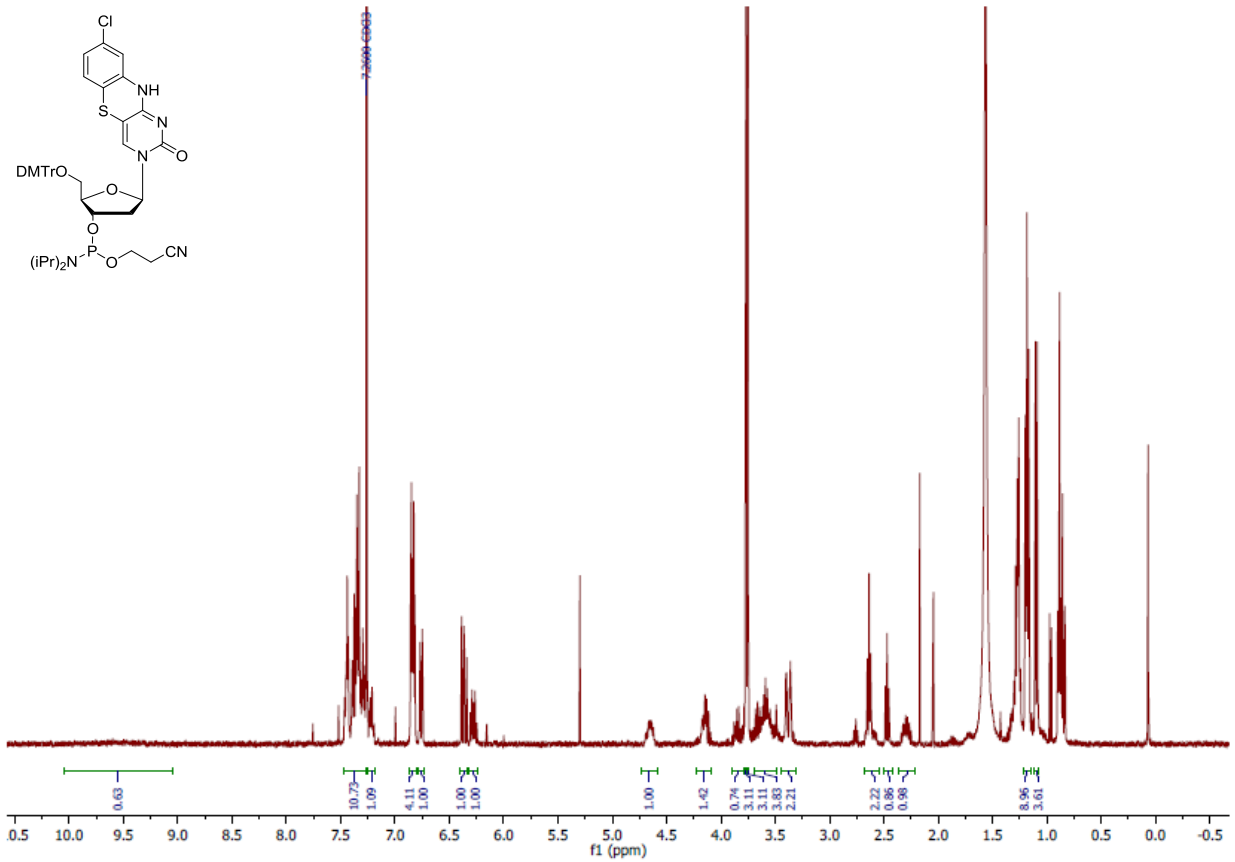

Figure S7. ^{1}H NMR of 8-Chloro-tC^{O} 2'-deoxy-5'-*O*-(4,4-dimethoxytrityl)-3'-O-[2-cyanoethoxy-(N,N-diisopropylamino)phosphino]-β-D-ribonucleoside. Spectrum acquired at 298 K, $CDCl_3$, 400 MHz.

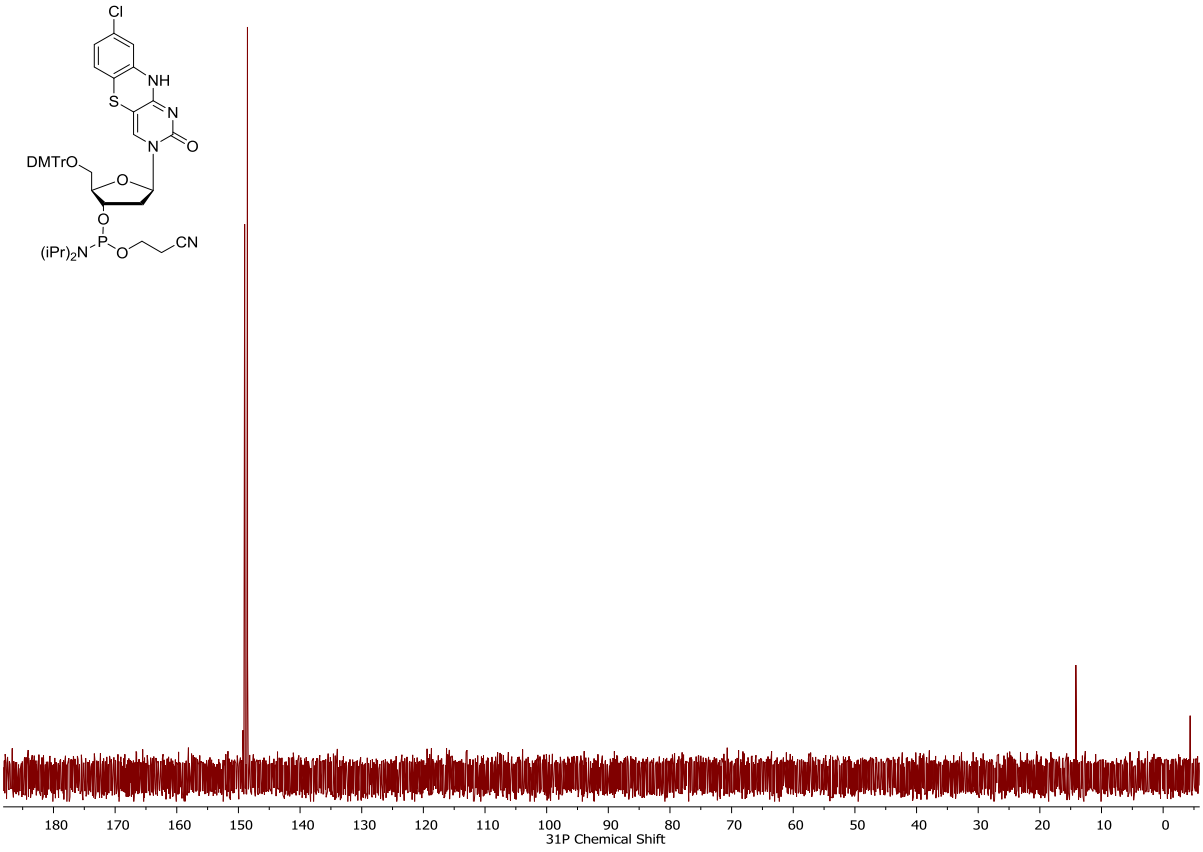

Figure S8. ^{31}P NMR of 8-Chloro-tC^{O} 2'-deoxy-5'-*O*-(4,4-dimethoxytrityl)-3'-O-[2-cyanoethoxy-(N,N-diisopropylamino)phosphino]-β-D-ribonucleoside. Spectrum acquired at 298 K, $CDCl_3$, 162 MHz.

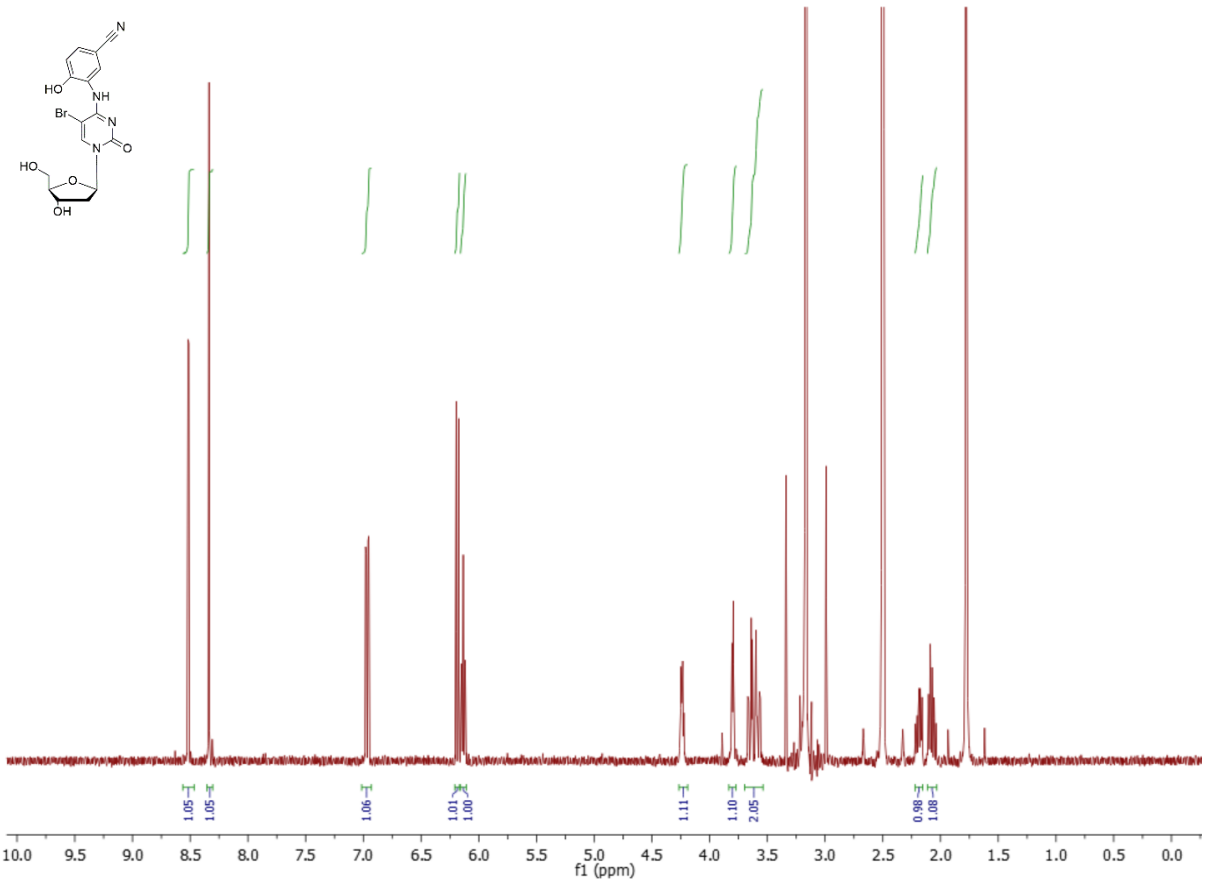

Figure S9. ^{1}H NMR of 5-Bromo-N4-(2-hydroxy-5-cyanophenyl)-2'-deoxycytidine. Spectrum acquired at 298 K, DMSO-d_6, 400 MHz.

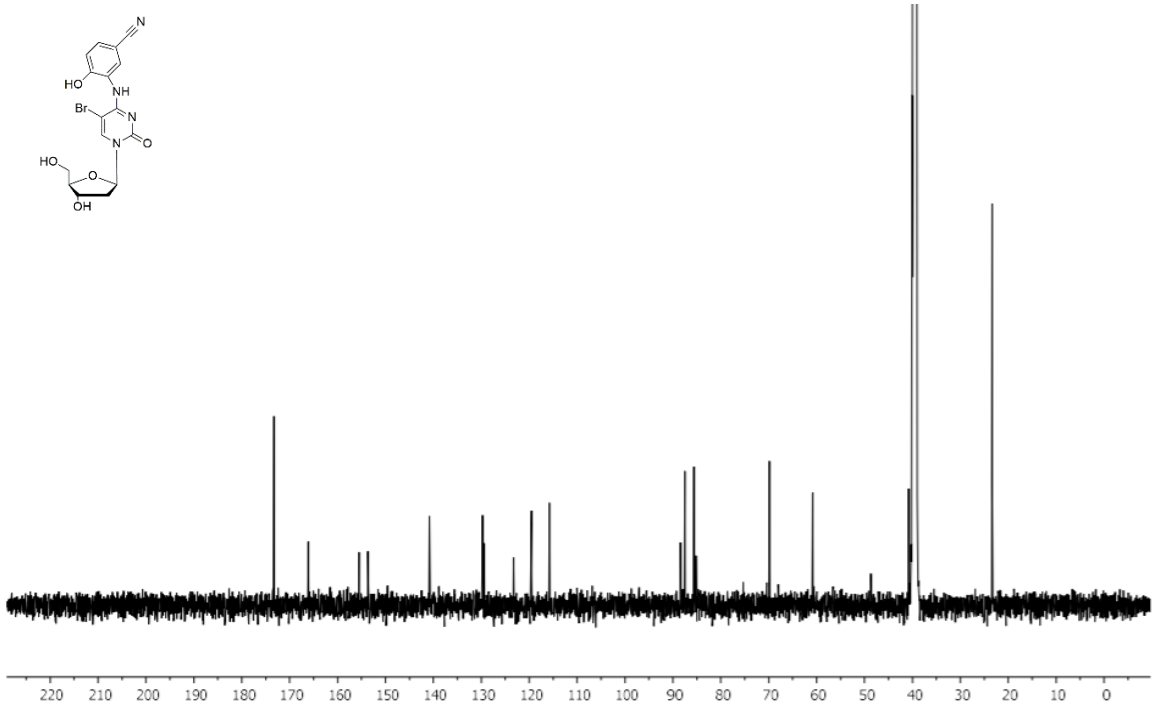

Figure S10. ^{13}C NMR of 5-Bromo-N4-(2-hydroxy-5-cyanophenyl)-2'-deoxycytidine. Spectrum acquired at 298 K $CDCl_3$, 100 MHz.

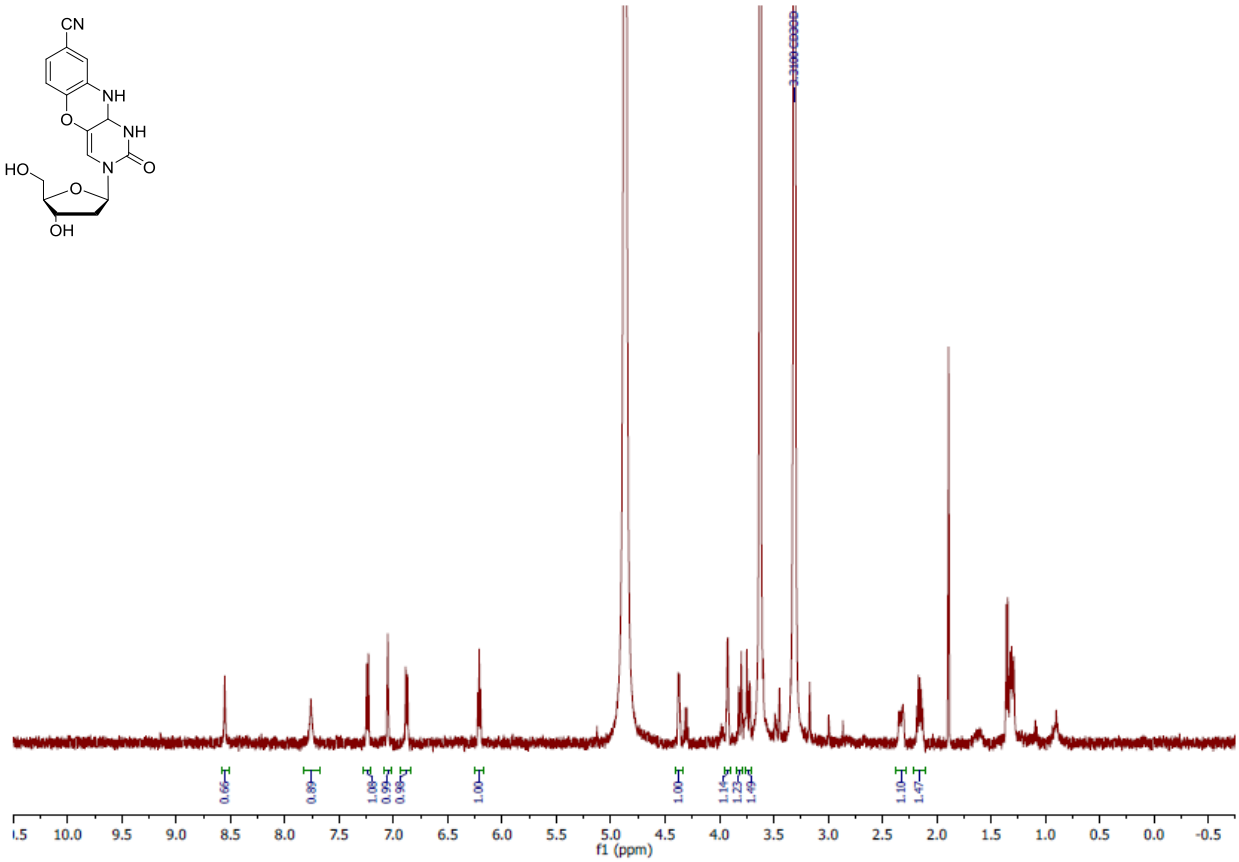

Figure S11. ^{1}H NMR of 8-Cyano-tC^{O} 2'-deoxy-β-$_{D}$-ribonucleoside, Spectrum acquired at 298 K, CD_3OD, 500 MHz.

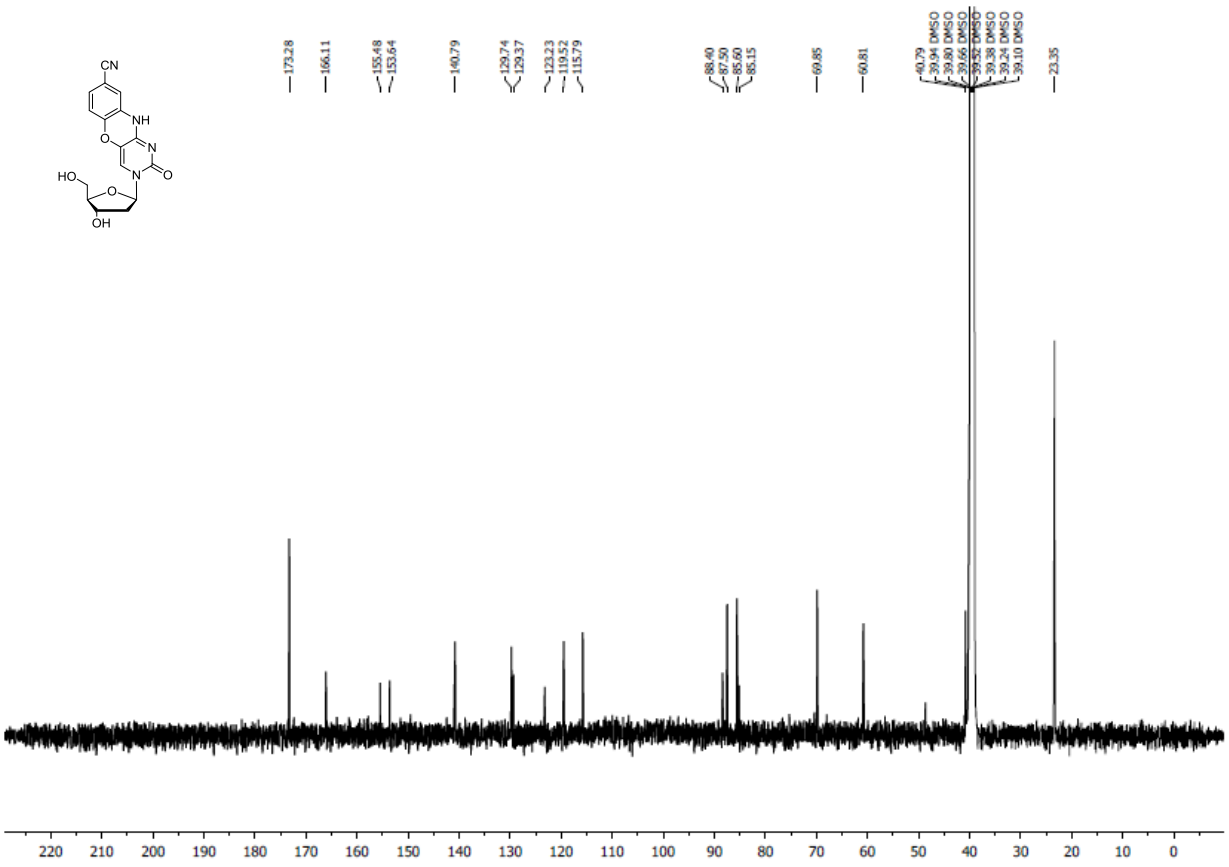

Figure S12. ^{13}C NMR of 8-Cyano-tC^{O} 2'-deoxy-β-$_{D}$-ribonucleoside, Spectrum acquired at 298 K, CD_3OD, 100 MHz.

4. Solid Phase Oligo Synthesis

Solid phase DNA synthesis to prepare oligonucleotides containing tC and tCo derivatives was performed by TriLink BioTechnologies, San Diego, CA using standard phosphoramidite conditions and tC and tCo amidites. The HPLC-purified oligonucleotides were characterized by MALDI-TOF mass spectrometry and found to match the expected molecular weights as shown below. Natural DNA oligonucleotides for the complementary sequences and the AA mismatch and AA complement with the dSpacer abasic site surrogate were obtained from Integrated DNA Technologies, Coralville, IA.

Parent tC:

Sequence Name	Sequence	Expected Molecular Weight (g/mol)	Mass Spec Analysis (amu)
AA	5'-CGC-A**A**X-**A**TC-G-3'	3104.0	3102.8

8-MeO-tC:

Sequence Name	Sequence	Expected Molecular Weight (g/mol)	Mass Spec Analysis (amu)
AA	5'-CGC-A**A**X-**A**TC-G-3'	3134.0	3132.8
GC	5'-CGC-A**G**X-**C**TC-G-3'	3126.0	3124.9
TA	5'-CGC-A**T**X-**A**TC-G-3'	3125.0	3123.7
TT	5'-CGC-T**T**X-**T**GC-G-3'	3131.9	3131.0

8-DEA-tC:

Sequence Name	Sequence	Expected Molecular Weight (g/mol)	Mass Spec Analysis (amu)
GA	5'-CGC-A**G**X-**A**TC-G-3'	3190.7	3190.1
CT	5'-CGC-A**C**X-**T**TC-G-3'	3141.8	3140.9
GC	5'-CGC-A**G**X-**C**TC-G-3'	3166.7	3166.5
CA	5'-CGC-A**C**X-**A**TC-G-3'	3150.8	3150.0
GG	5'-CGC-A**G**X-**G**TC-G-3'	3206.7	3206.2
CC	5'-CGC-A**C**X-**C**TC-G-3'	3126.8	3126.0
TA	5'-CGC-A**T**X-**A**TC-G-3'	3165.8	3165.2
TT	5'-CGC-A**T**X-**T**TC-G-3'	3156.8	3156.1
AA	5'-CGC-A**A**X-**A**TC-G-3'	3174.8	3174.2

8-Cl-tC^{o}:

Sequence Name	Sequence	Expected Molecular Weight (g/mol)	Mass Spec Analysis (amu)
AA	5'-CGC-A**A**X-**A**TC-G-3'	3121.8	3121.1
GC	5'-CGC-A**G**X-**C**TC-G-3'	3113.7	3113.4
TA	5'-CGC-A**T**X-**A**TC-G-3'	3112.8	3112.3
TT	5'-CGC-T**T**X-**T**GC-G-3'	3119.7	3119.2

Complementary Sequences

Sequence Name	Sequence
GA complement	5'-CGA-TGC-TGC-G-3'
CT complement	5'-CGA-AGG-TGC-G-3'
GC complement	5'-CGA-GGC-TGC-G-3'
CA complement	5'-CGA-TGG-TGC-G-3'
GG complement	5'-CGA-CGC-TGC-G-3'
CC complement	5'-CGA-GGG-TGC-G-3'
TA complement	5'-CGA-TGA-TGC-G-3'
TT complement	5'-CGA-AGA-TGC-G-3'
AA complement	5'-CGA-TGT-TGC-G-3'
AA mismatch complement	5'-CGA-TAT-TGC-G-3'
AA abasic site complement	5'-CGA-T(dSpacer)T-TGC-G-3'

5. Quantum Yield Determinations

All photophysical experiments were measured in a quartz sub-micro cuvette (10 mm path length) purchased from Starnacell Inc. Solutions were prepared in 1X PBS buffer at pH 7.4. Steady state emission scans were recorded using a PTI QuantaMaster QM-400 and absorbances were measured on a Shimadzu UV-1700 Pharmaspec spectrometer. Quantum yield measurements were performed using the comparative method of Williams *et al.* and measured in duplicate, at minimum.[15] Quinine sulfate in 0.1M H_2SO_4 was used as a reference standard for all photophysical measurements. We validated the measurements by using a commercial sample of pyrrolo-dC and obtaining a fluorescence quantum yield of 0.046, matching the value of 0.05 as reported by the Tor group.[16] All measurements were taken with an absorbance range of 0.01-0.1. Subsequent dilutions were performed stepwise in order to obtain a minimum of five absorbance and emission spectra for quantum yield determinations. *Representative data from these quantum yield measurements is plotted below.* Quantum yield determinations were obtained using the following equation:

$$\Phi_{\mathrm{X}} = \Phi_{\mathrm{Std}} \left(\frac{\mathrm{Slope_X}}{\mathrm{Slope_{Std}}} \right) \left(\frac{{\eta_{\mathrm{X}}}^2}{{\eta_{\mathrm{Std}}}^2} \right)$$

The determination of quantum yields for single-stranded oligonucleotides containing 8-DEA-tC were calculated using the integrated emission intensity measurements of the single strand prior to the addition of the complementary strand, with the following equation. This method was validated by comparison with and confirmed with a SS quantum yield experiment.

$$SS\ \Phi = DS\ \Phi\ \times \frac{SS\ EMInitial}{DS\ EMInitial} \times \frac{DS\ ABS}{SS\ ABS} \times \frac{DS\ Total\ Vol}{SS\ Total\ Vol}$$

Samples of double-stranded oligonucleotides were prepared using a known concentration of single-stranded oligonucleotide and adding a total of 2.4 equivalents of complementary strand at room temperature. A single-strand absorbance and emission were taken prior to the addition of the first 1.2 equivalents of complementary strand for purposes of single-strand calculation and verification of hybridization. An additional 1.2 equivalent is added after the first double-strand to ensure that complete hybridization was achieved. Thermal annealing procedures had no effect on the measurements as expected, given that these sequences were chosen to have no competing, stable secondary structures.

Normalized absorption and emission plots of single-stranded oligonucleotides and double-stranded oligonucleotides in 1X PBS buffer at pH 7.4 are shown below. Note: ***Not all normalized quantum yields are drawn to the same scale.***

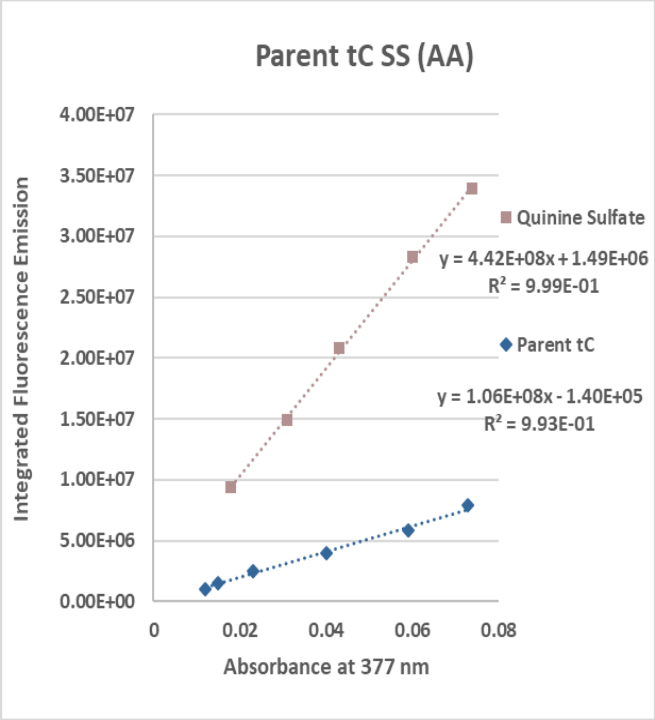

Quinine Sulfate		tC SS (AA)	
Absorbance (377 nm)	Integrated Emission	Absorbance (377 nm)	Integrated Emission
0.074	3.39E+07	0.073	7.87E+06
0.060	2.83E+07	0.059	5.80E+06
0.043	2.08E+07	0.04	4.02E+06
0.031	1.49E+07	0.023	2.54E+06
0.018	9.43E+06	0.015	1.50E+06
		0.012	1.02E+06

Figure S13. Quantum Yield determination plot and data table of Parent tC SS (AA) in 1X PBS Buffer at 23°C.

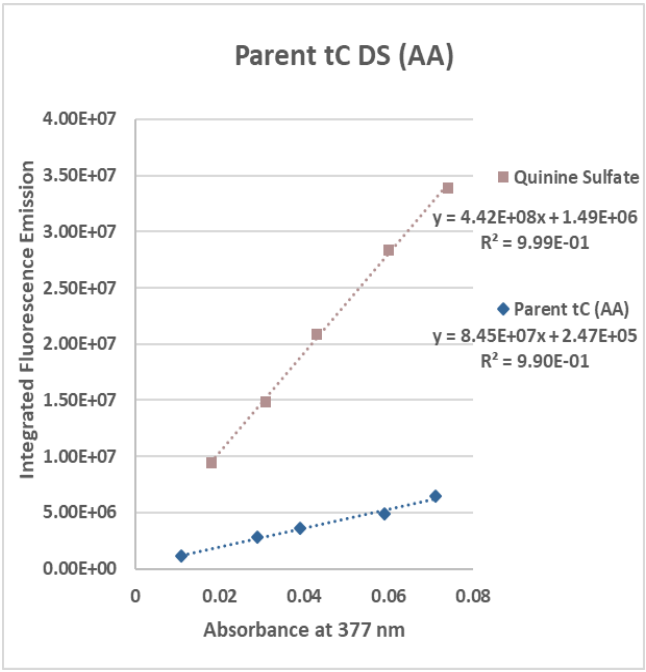

Quinine Sulfate		tC DS (AA)	
Absorbance (377 nm)	Integrated Emission	Absorbance (377 nm)	Integrated Emission
0.074	3.39E+07	0.071	6.43E+06
0.060	2.83E+07	0.059	4.91E+06
0.043	2.08E+07	0.039	3.59E+06
0.031	1.49E+07	0.029	2.85E+06
0.018	9.43E+06	0.011	1.11E+06

Figure S14. Quantum Yield determination plot and data table of Parent tC DS (AA) in 1X PBS Buffer at 23°C.

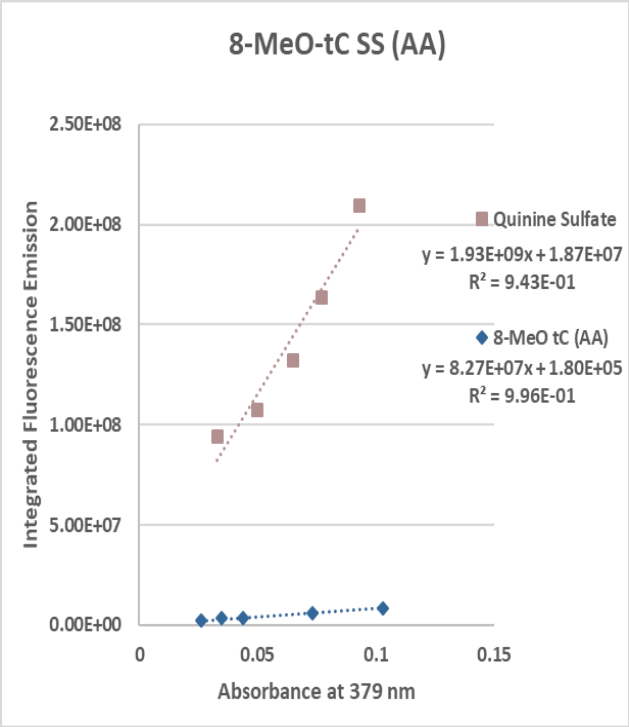

Quinine Sulfate		8-MeO-tC SS (AA)	
Absorbance (379 nm)	Integrated Emission	Absorbance (379 nm)	Integrated Emission
0.093	2.09E+08	0.103	8.68E+06
0.077	1.63E+08	0.073	6.25E+06
0.065	1.32E+08	0.044	3.70E+06
0.050	1.08E+08	0.035	3.34E+06
0.033	9.44E+07	0.026	2.18E+06

Figure S15. Quantum Yield determination plot and data table of 8-MeO-tC SS (AA) in 1X PBS Buffer at 23°C.

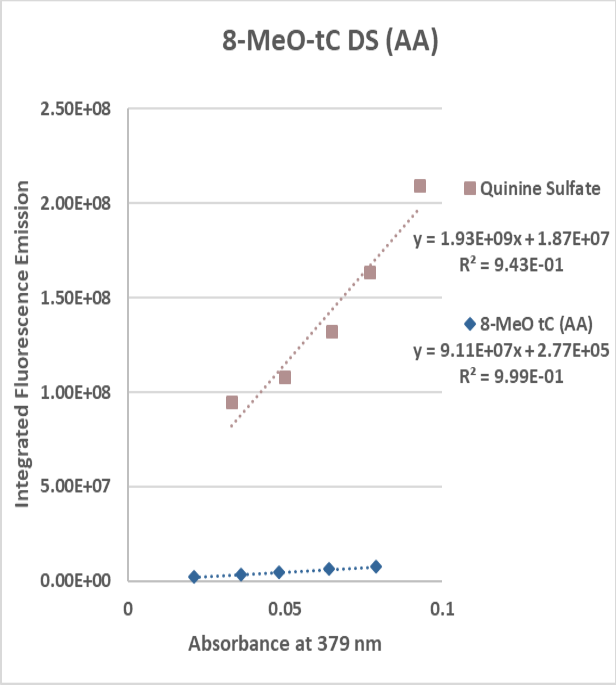

Quinine Sulfate		8-MeO-tC DS (AA)	
Absorbance (379 nm)	Integrated Emission	Absorbance (379 nm)	Integrated Emission
0.093	2.09E+08	0.079	7.40E+06
0.077	1.63E+08	0.064	6.18E+06
0.065	1.32E+08	0.048	4.68E+06
0.050	1.08E+08	0.036	3.61E+06
0.033	9.44E+07	0.021	2.12E+06

Figure S16. Quantum Yield determination plot and data table of 8-MeO-tC DS (AA) in 1X PBS Buffer at 23°C.

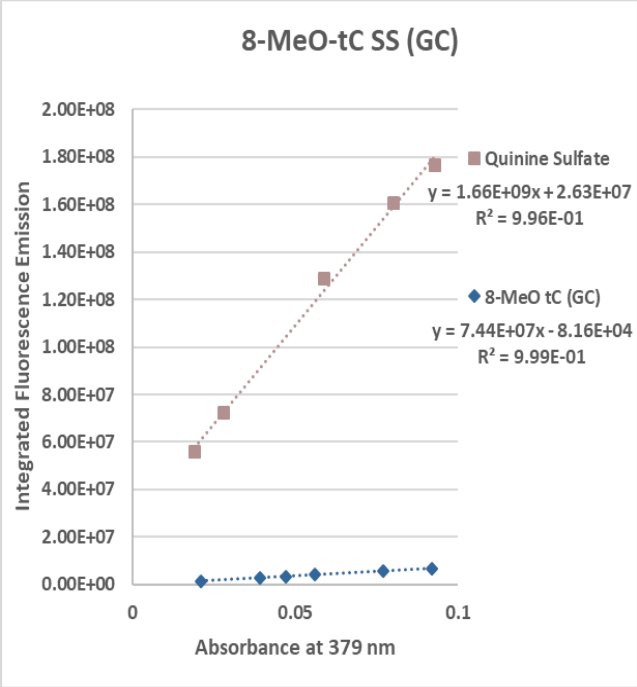

Quinine Sulfate		8-MeO-tC SS (GC)	
Absorbance (379 nm)	Integrated Emission	Absorbance (379 nm)	Integrated Emission
0.093	1.77E+08	0.092	6.72E+06
0.080	1.61E+08	0.077	5.67E+06
0.059	1.29E+08	0.056	4.18E+06
0.028	7.22E+07	0.047	3.36E+06
0.019	5.57E+07	0.039	2.78E+06
		0.021	1.49E+06

Figure S17. Quantum Yield determination plot and data table of 8-MeO tC SS (GC) in 1X PBS Buffer at 23°C.

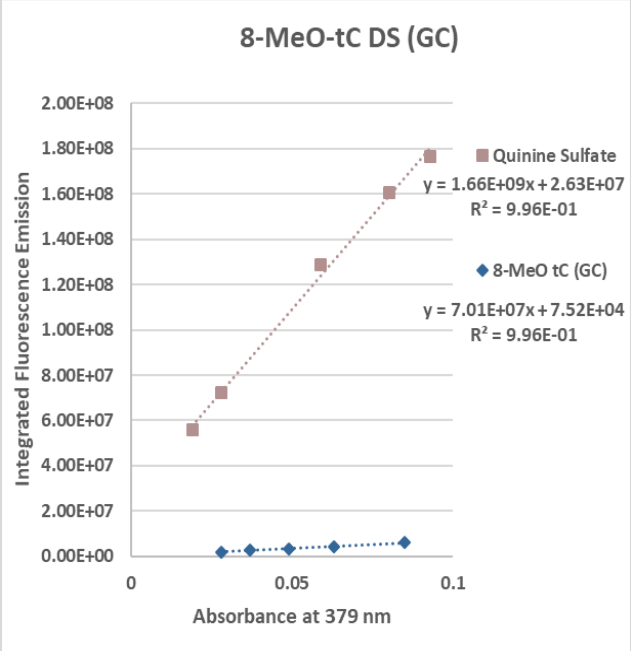

Quinine Sulfate		8-MeO-tC DS (GC)	
Absorbance (379 nm)	Integrated Emission	Absorbance (379 nm)	Integrated Emission
0.093	1.77E+08	0.085	6.08E+06
0.080	1.61E+08	0.063	4.42E+06
0.059	1.29E+08	0.049	3.44E+06
0.028	7.22E+07	0.037	2.81E+06
0.019	5.57E+07	0.028	1.99E+06

Figure S18. Quantum Yield determination plot and data table of 8-MeO-tC DS (GC) 1X PBS Buffer at 23°C.

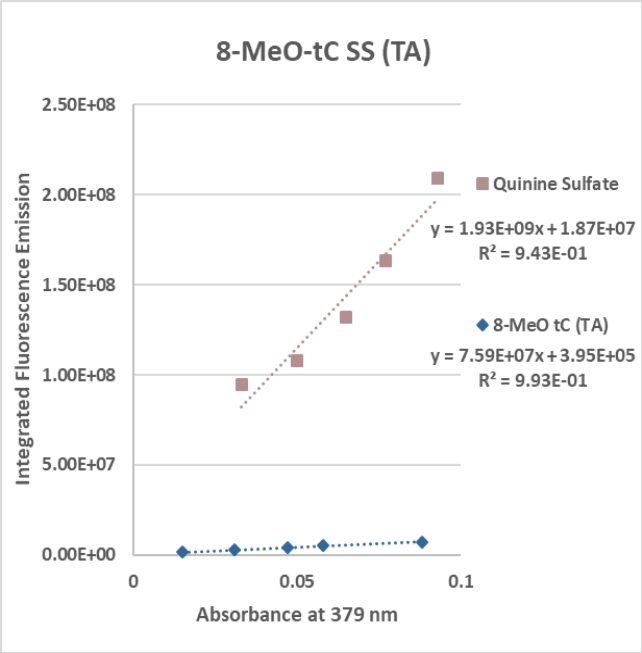

Quinine Sulfate		8-MeO-tC SS (TA)	
Absorbance (379 nm)	Integrated Emission	Absorbance (379 nm)	Integrated Emission
0.093	2.09E+08	0.088	6.90E+06
0.077	1.63E+08	0.058	4.97E+06
0.065	1.32E+08	0.047	4.13E+06
0.050	1.08E+08	0.031	2.76E+06
0.033	9.44E+07	0.015	1.36E+06

Figure S19. Quantum Yield determination plot and data table of 8-MeO-tC SS (TA) in 1X PBS Buffer at 23°C.

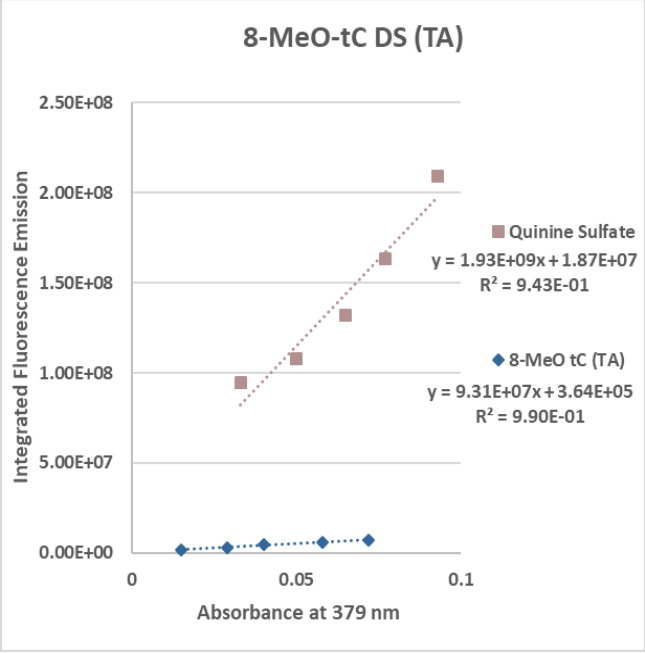

Quinine Sulfate		8-MeO-tC DS (TA)	
Absorbance (379 nm)	Integrated Emission	Absorbance (379 nm)	Integrated Emission
0.093	2.09E+08	0.072	7.05E+06
0.077	1.63E+08	0.058	5.58E+06
0.065	1.32E+08	0.040	4.46E+06
0.050	1.08E+08	0.029	3.01E+06
0.033	9.44E+07	0.015	1.64E+06

Figure S20. Quantum Yield determination plot and data table of 8-MeO-tC DS (TA) 1X PBS Buffer at 23°C.

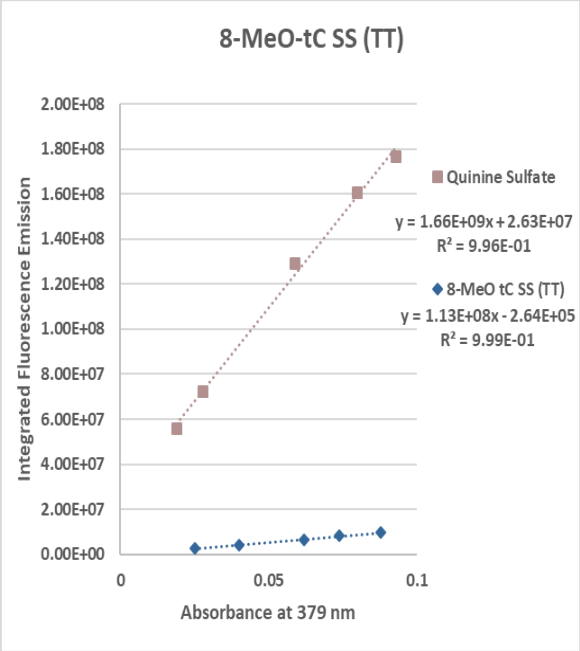

Quinine Sulfate		8-MeO-tC SS (TT)	
Absorbance (379 nm)	Integrated Emission	Absorbance (379 nm)	Integrated Emission
0.093	1.77E+08	0.088	9.61E+06
0.080	1.61E+08	0.074	8.24E+06
0.059	1.29E+08	0.062	6.62E+06
0.028	7.22E+07	0.040	4.19E+06
0.019	5.57E+07	0.025	2.61E+06

Figure S21. Quantum Yield determination plot and data table of 8-MeO-tC SS (TT) in 1X PBS Buffer at 23°C.

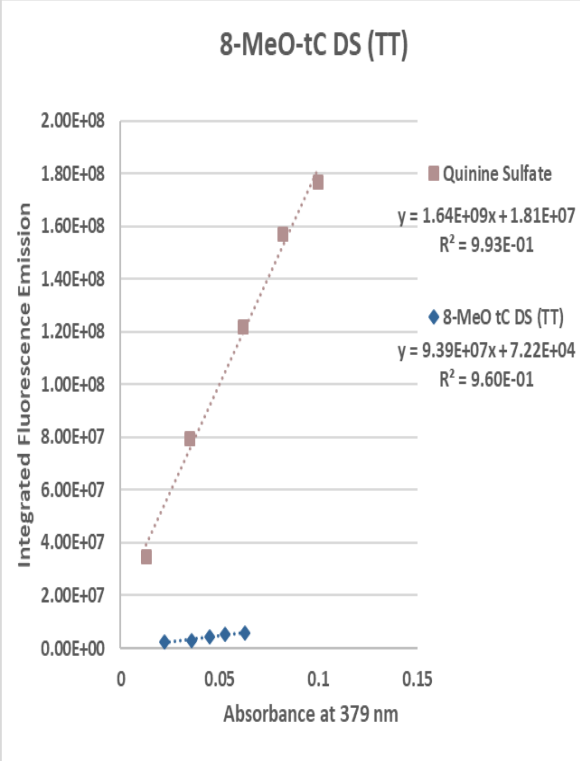

Quinine Sulfate		8-MeO-tC DS (TT)	
Absorbance (379 nm)	Integrated Emission	Absorbance (379 nm)	Integrated Emission
0.100	1.77E+08	0.063	5.82E+06
0.082	1.57E+08	0.053	5.46E+06
0.062	1.22E+08	0.045	4.25E+06
0.035	7.95E+07	0.036	3.09E+06
0.013	3.49E+07	0.022	2.29E+06

Figure S22. Quantum Yield determination plot and data table of 8-MeO-tC DS (TT) 1X PBS Buffer at 23°C.

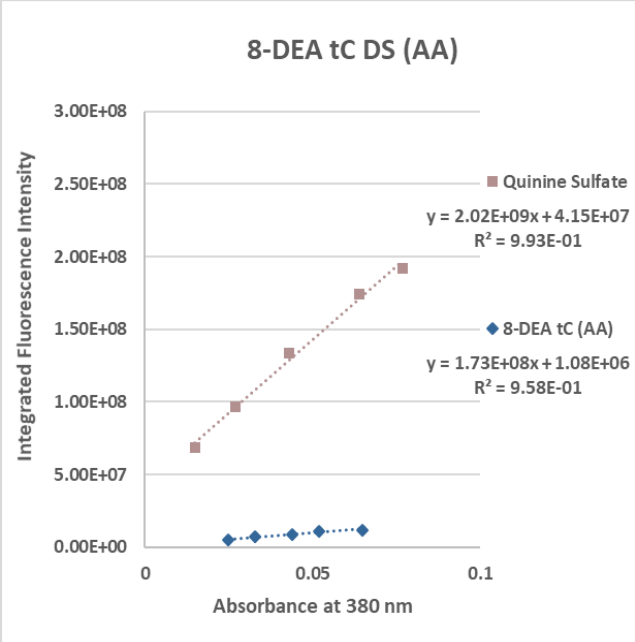

Quinine Sulfate		8-DEA tC (AA)	
Absorbance (380 nm)	Integrated Emission	Absorbance (380 nm)	Integrated Emission
0.077	1.92E+08	0.077	1.18E+08
0.064	1.74E+08	0.064	7.31E+08
0.043	1.33E+08	0.043	2.82E+08
0.027	9.63E+07	0.027	1.96E+07
0.015	6.83E+07	0.015	1.21E+07

Figure S23. Quantum Yield determination plot and data table of 8-DEA tC DS (AA) in 1X PBS Buffer at 23°C.

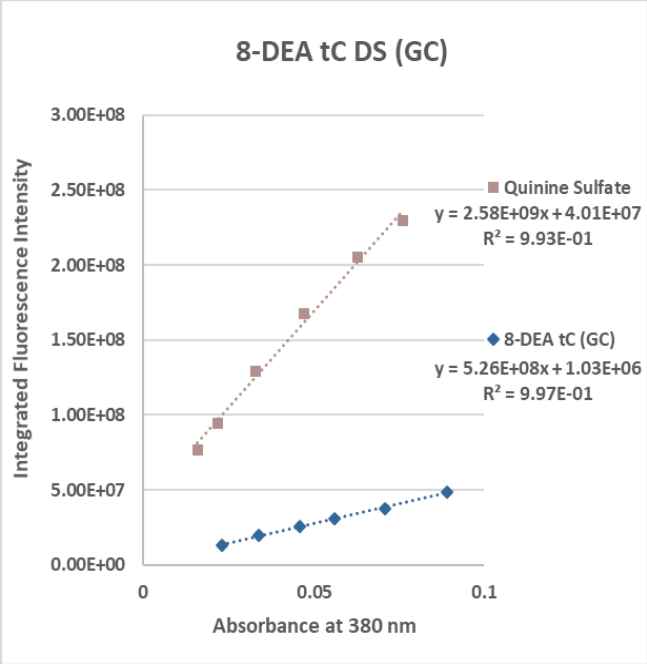

Quinine Sulfate		8-DEA tC (GC)	
Absorbance (380 nm)	Integrated Emission	Absorbance (380 nm)	Integrated Emission
0.076	2.30E+08	0.089	4.86E+07
0.063	2.05E+08	0.071	3.72E+07
0.047	1.68E+08	0.056	3.06E+07
0.033	1.29E+08	0.046	2.53E+07
0.022	9.47E+07	0.034	1.94E+07
0.028	7.67E+07	0.025	1.30E+07

Figure S24. Quantum Yield determination plot and data table of 8-DEA tC DS (GC) in 1X PBS Buffer at 23°C.

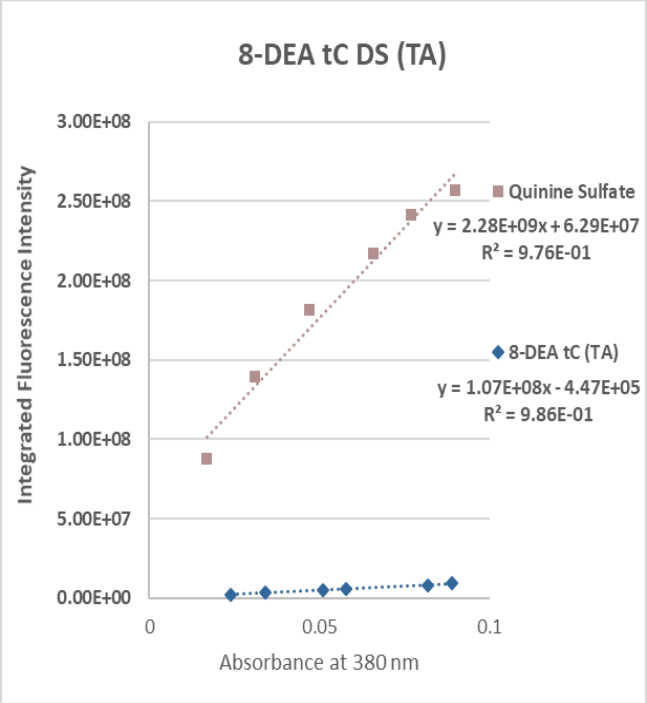

Quinine Sulfate		8-DEA tC (TA)	
Absorbance (380 nm)	Integrated Emission	Absorbance (380 nm)	Integrated Emission
0.090	2.57E+08	0.089	9.62E+06
0.077	2.41E+08	0.082	7.84E+06
0.066	2.17E+08	0.058	5.76E+06
0.047	1.82E+08	0.051	4.92E+06
0.031	1.40E+08	0.034	3.22E+06
0.017	8.81E+07	0.024	2.24E+06

Figure S25. Quantum Yield determination plot and data table of 8-DEA tC DS (TA) in 1X PBS Buffer at 23°C.

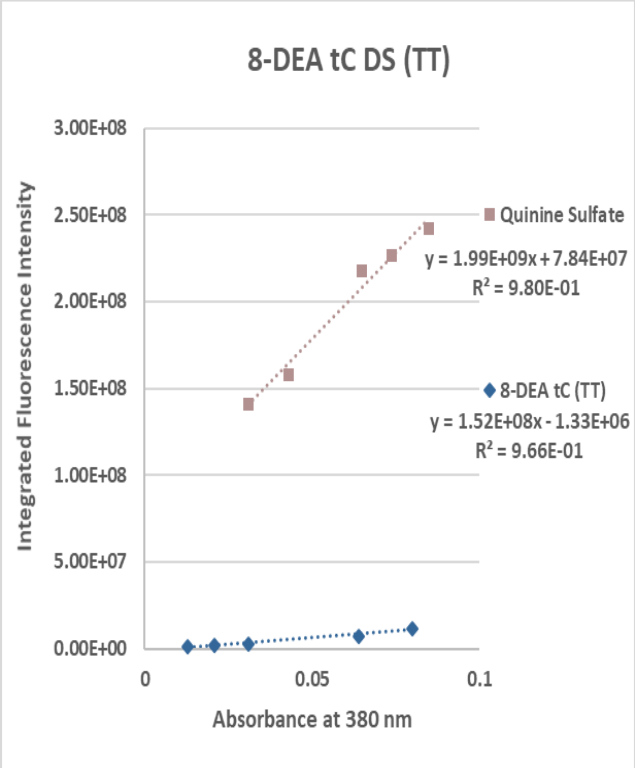

Quinine Sulfate		8-DEA tC (TT)	
Absorbance (380 nm)	Integrated Emission	Absorbance (380 nm)	Integrated Emission
0.085	2.42E+08	0.080	1.18E+07
0.074	2.27E+08	0.064	7.31E+06
0.065	2.17E+08	0.031	2.82E+06
0.043	1.58E+08	0.021	1.96E+06
0.031	1.41E+08	0.013	1.21E+06

Figure S26. Quantum Yield determination plot and data table of 8-DEA tC DS (TT) in 1X PBS Buffer at 23°C.

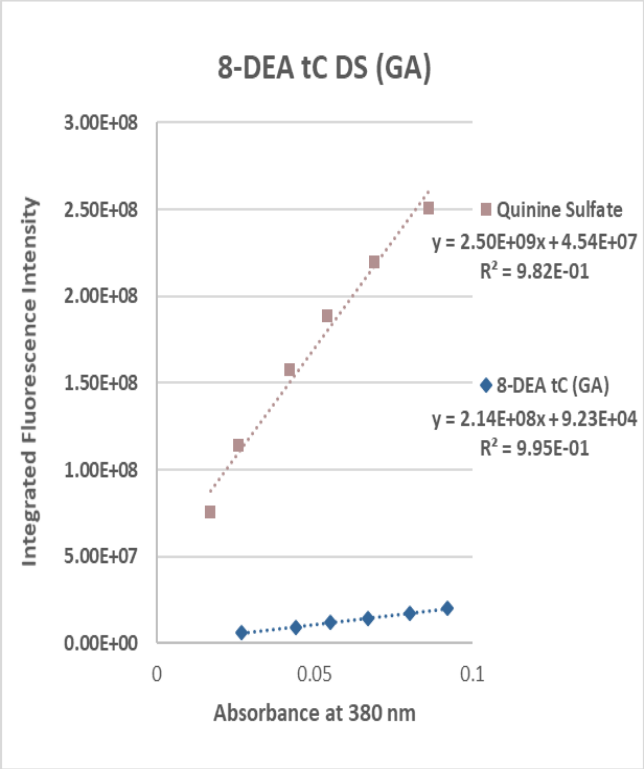

Quinine Sulfate		8-DEA tC (GA)	
Absorbance (380 nm)	Integrated Emission	Absorbance (380 nm)	Integrated Emission
0.086	2.51E+08	0.092	2.03E+07
0.069	2.19E+08	0.08	1.70E+07
0.054	1.89E+08	0.067	1.42E+07
0.042	1.58E+08	0.055	1.19E+07
0.026	1.14E+08	0.044	9.19E+07
0.017	7.54E+07	0.027	7.54E+07

Figure S27. Quantum Yield determination plot and data table of 8-DEA tC DS (GA) in 1X PBS Buffer at 23°C.

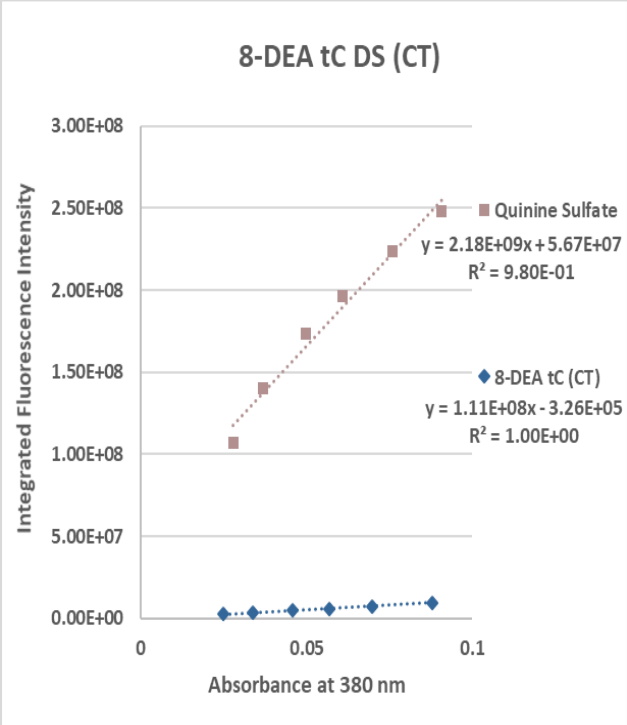

Quinine Sulfate		8-DEA tC (CT)	
Absorbance (380 nm)	Integrated Emission	Absorbance (380 nm)	Integrated Emission
0.091	2.48E+08	0.088	9.37E+06
0.076	2.24E+08	0.070	7.50E+06
0.061	1.96E+08	0.057	5.97E+06
0.050	1.73E+08	0.046	4.69E+06
0.037	1.40E+08	0.034	3.42E+06
0.028	1.07E+08	0.025	2.48E+06

Figure S28. Quantum Yield determination plot and data table of 8-DEA tC DS (CT) in 1X PBS Buffer at 23°C.

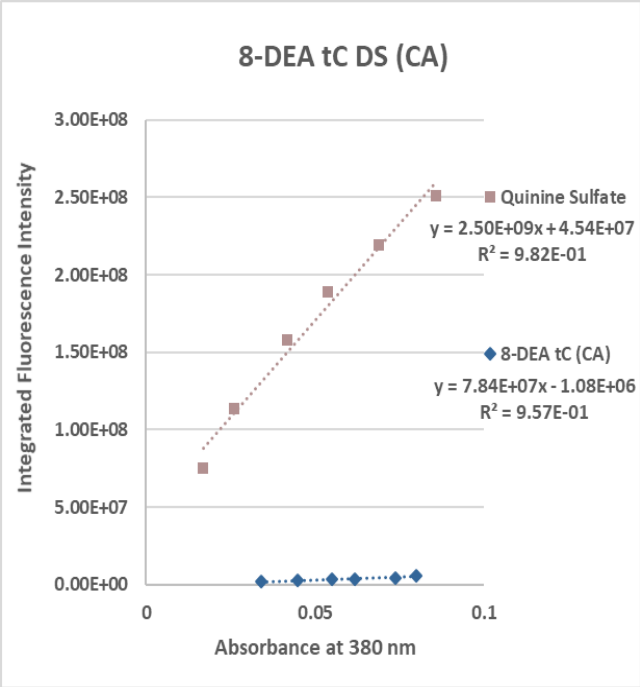

Quinine Sulfate		8-DEA tC (CA)	
Absorbance (380 nm)	Integrated Emission	Absorbance (380 nm)	Integrated Emission
0.086	2.51E+08	0.080	5.66E+06
0.069	2.19E+08	0.074	4.35E+06
0.054	1.89E+08	0.062	3.66E+06
0.042	1.58E+08	0.055	3.15E+06
0.026	1.14E+08	0.045	2.39E+06
0.017	7.54E+07	0.034	1.78E+06

Figure S29. Quantum Yield determination plot and data table of 8-DEA tC DS (CA) in 1X PBS Buffer at 23°C.

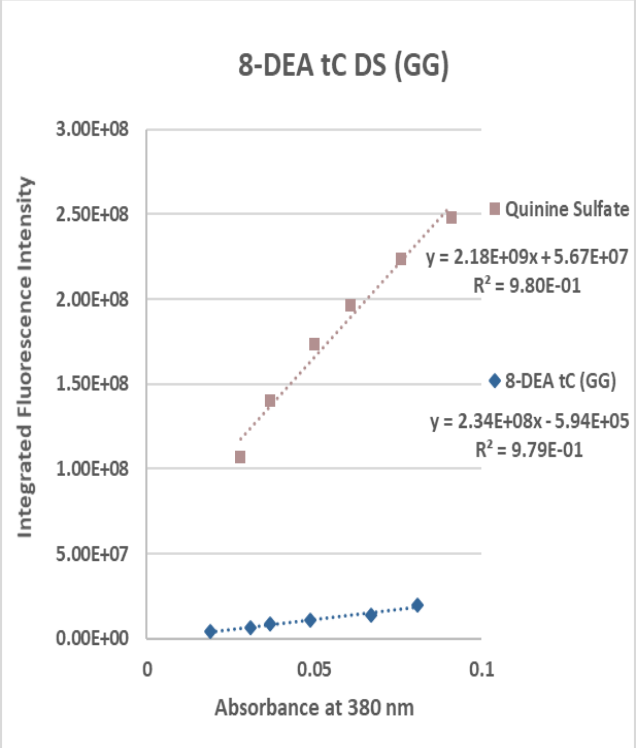

Quinine Sulfate		8-DEA tC (GG)	
Absorbance (380 nm)	Integrated Emission	Absorbance (380 nm)	Integrated Emission
0.091	2.48E+08	0.081	1.95E+07
0.076	2.24E+08	0.067	1.39E+07
0.061	1.96E+08	0.049	1.05E+07
0.050	1.73E+08	0.037	8.26E+06
0.037	1.40E+08	0.031	6.42E+06
0.028	1.07E+08	0.019	4.40E+06

Figure S30. Quantum Yield determination plot and data table of 8-DEA tC DS (GG) in 1X PBS Buffer at 23°C.

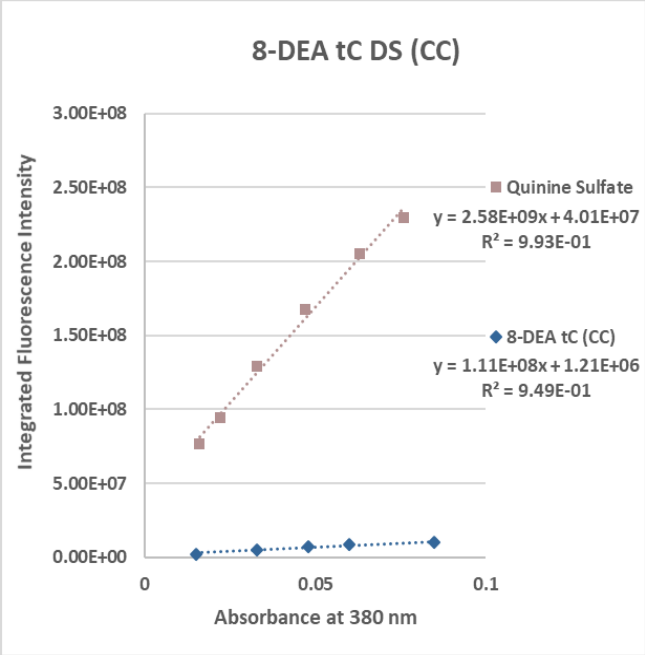

Quinine Sulfate		8-DEA tC (CC)	
Absorbance (380 nm)	Integrated Emission	Absorbance (380 nm)	Integrated Emission
0.091	2.48E+08	0.081	1.95E+07
0.076	2.24E+08	0.067	1.39E+07
0.061	1.96E+08	0.049	1.05E+07
0.050	1.73E+08	0.037	8.26E+06
0.037	1.40E+08	0.031	6.42E+06
0.028	1.07E+08	0.019	4.40E+06

Figure S31. Quantum Yield determination plot and data table of 8-DEA tC DS (CC) in 1X PBS Buffer at 23°C.

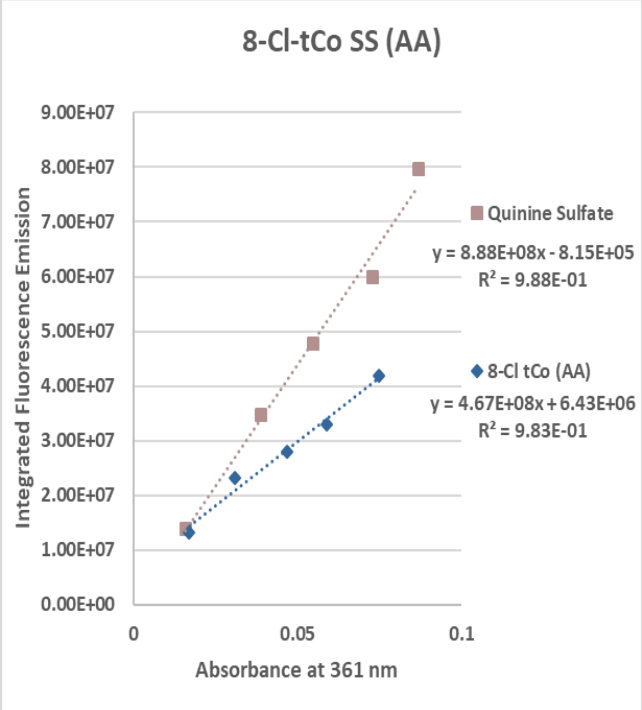

Quinine Sulfate		8-Cl-tC^{o} SS (AA)	
Absorbance (361 nm)	Integrated Emission	Absorbance (361 nm)	Integrated Emission
0.087	7.98E+07	0.075	4.18E+07
0.073	5.98 E+07	0.059	3.31E+07
0.055	4.77E+07	0.047	2.79E+07
0.039	3.47E+07	0.031	2.32E+07
0.016	1.38E+07	0.017	1.31E+07

Figure S32. Quantum Yield determination plot and data table of 8-Cl-tC^{O} SS (AA) in 1X PBS Buffer at 23°C.

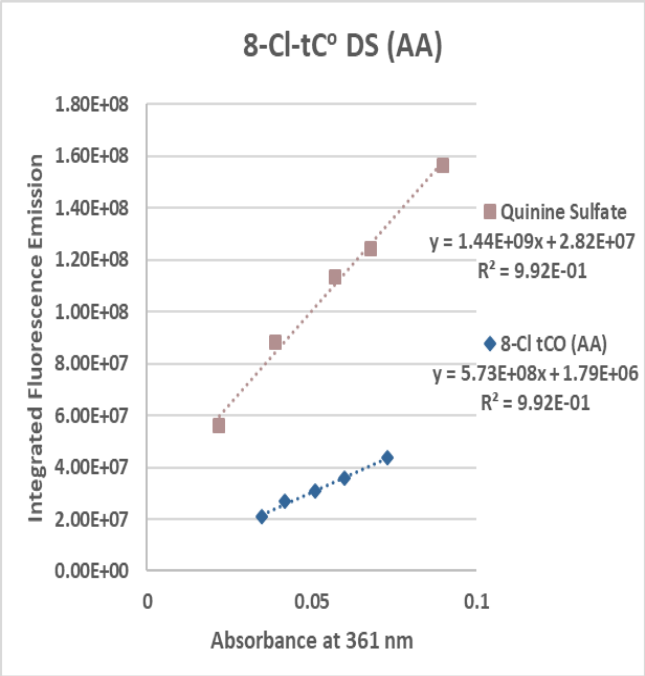

Quinine Sulfate		8-Cl-tC° DS (AA)	
Absorbance (361 nm)	Integrated Emission	Absorbance (361 nm)	Integrated Emission
0.090	1.57E+08	0.073	4.37E+07
0.068	1.24E+08	0.060	3.59E+07
0.057	1.14E+08	0.051	3.08E+07
0.039	8.81E+07	0.042	2.71E+07
0.022	5.62E+07	0.035	2.10E+07

Figure S33. Quantum Yield determination plot and data table of 8-Cl-tC^{O} DS (AA) in 1X PBS Buffer at 23°C.

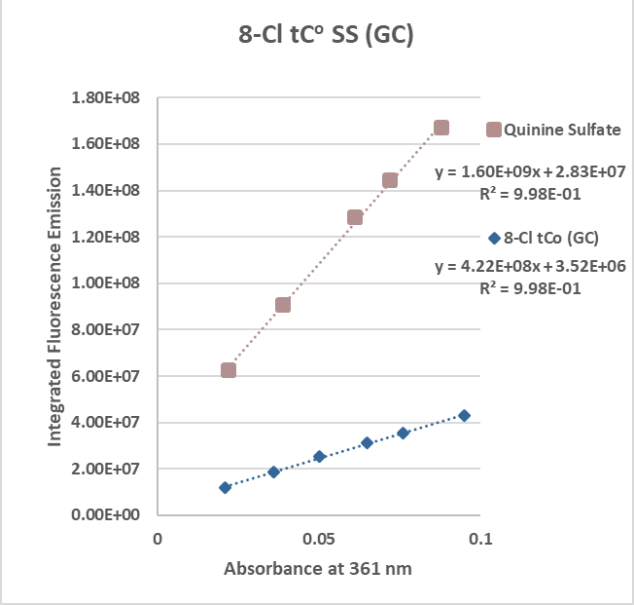

Quinine Sulfate		8-Cl-tC° SS (GC)	
Absorbance (361 nm)	Integrated Emission	Absorbance (361 nm)	Integrated Emission
0.088	1.67E+08	0.095	4.31E+07
0.072	1.44E+08	0.076	3.55E+07
0.061	1.28E+08	0.065	3.14E+07
0.039	9.08E+07	0.050	2.52E+07
0.022	6.23E+07	0.036	1.88E+07
		0.021	1.17E+07

Figure S34. Quantum Yield determination plot and data table of 8-Cl-tC^{O} SS (GC) in 1X PBS Buffer at 23°C.

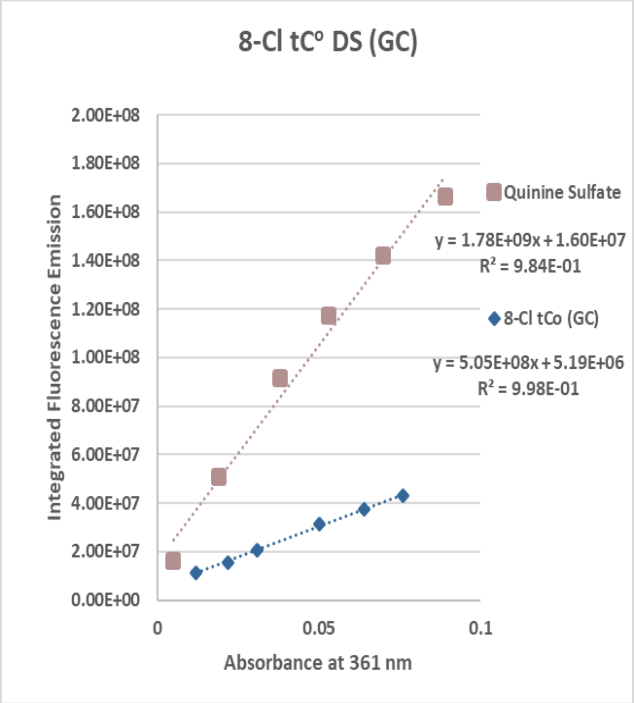

Quinine Sulfate		8-Cl-tC° DS (GC)	
Absorbance (361 nm)	Integrated Emission	Absorbance (361 nm)	Integrated Emission
0.089	1.66E+08	0.076	4.32E+07
0.07	1.42E+08	0.064	3.75E+07
0.053	1.17E+08	0.05	3.13E+07
0.038	9.14E+07	0.031	2.07E+07
0.019	5.09E+07	0.022	1.57E+07
0.005	1.61E+07	0.012	1.15E+07

Figure S35. Quantum Yield determination plot and data table of 8-Cl-tC° DS (GC) in 1X PBS Buffer at 23°C.

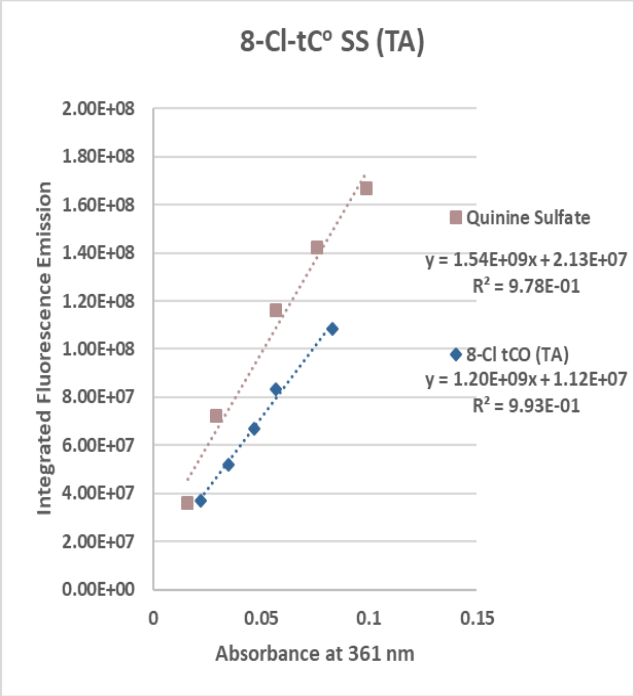

Quinine Sulfate		8-Cl-tC° SS (TA)	
Absorbance (361 nm)	Integrated Emission	Absorbance (361 nm)	Integrated Emission
0.099	1.67E+08	0.083	1.09E+08
0.076	1.42E+08	0.057	8.33E+07
0.057	1.16E+08	0.047	6.69E+07
0.029	7.23E+07	0.035	5.19E+07
0.016	3.61E+07	0.022	3.70E+07

Figure S36. Quantum Yield determination plot and data table of 8-Cl-tC° SS (TA) in 1X PBS Buffer at 23°C.

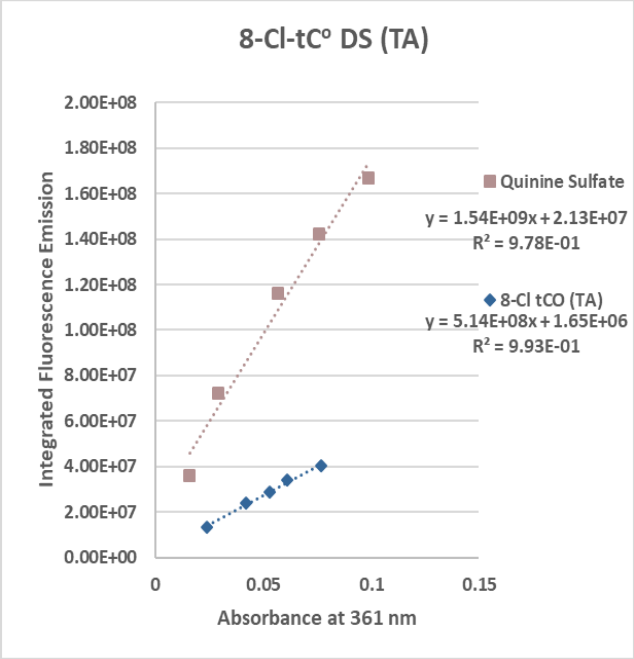

Quinine Sulfate		8-Cl-tC° DS (TA)	
Absorbance (361 nm)	Integrated Emission	Absorbance (361 nm)	Integrated Emission
0.099	1.67E+08	0.077	4.04E+07
0.076	1.42E+08	0.061	3.39E+07
0.057	1.16E+08	0.053	2.88E+07
0.029	7.23E+07	0.042	2.42E+07
0.016	3.61E+07	0.024	1.32E+07

Figure S37. Quantum Yield determination plot and data table of 8-Cl-tC^{O} DS (TA) 1X PBS Buffer at 23°C.

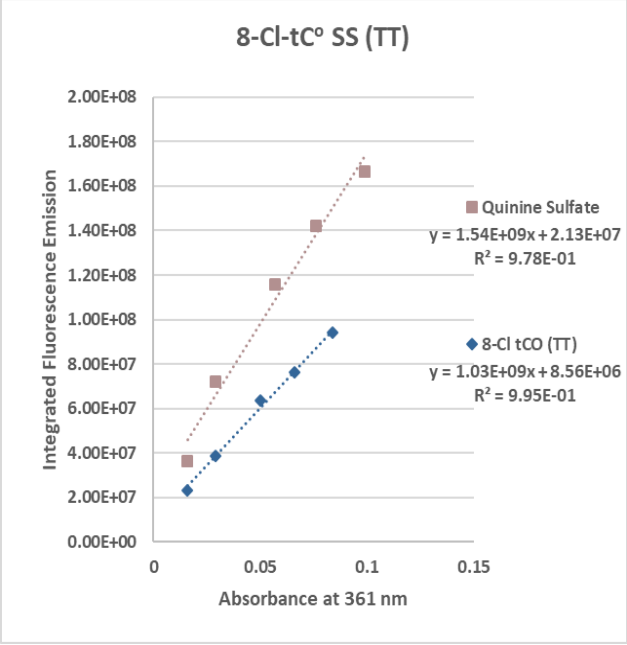

Quinine Sulfate		8-Cl-tC° SS (TT)	
Absorbance (361 nm)	Integrated Emission	Absorbance (361 nm)	Integrated Emission
0.099	1.67E+08	0.084	9.42E+07
0.076	1.42E+08	0.066	7.62E+07
0.057	1.16E+08	0.050	6.35E+07
0.029	7.23E+07	0.029	3.88E+07
0.016	3.61E+07	0.016	2.34E+07

Figure S38. Quantum Yield determination plot and data table of 8-Cl-tC^{O} SS (TT) in 1X PBS Buffer at 23°C.

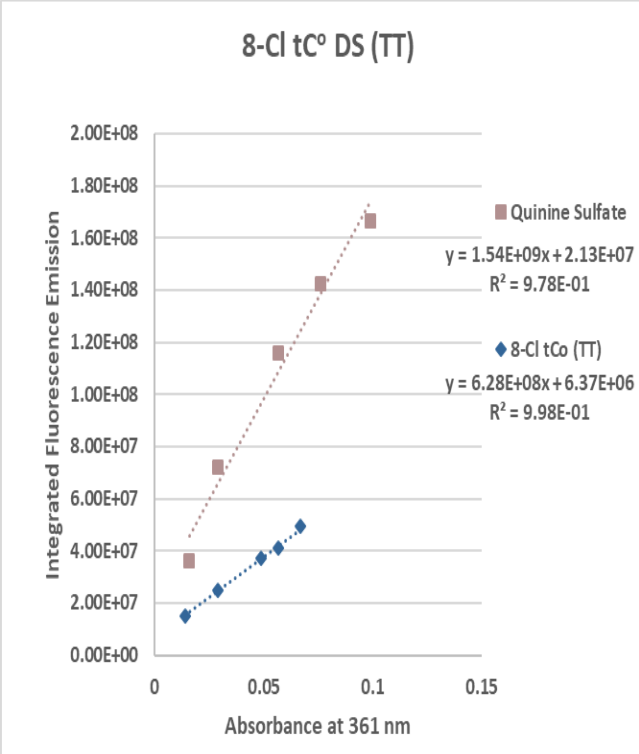

Quinine Sulfate		8-Cl tC° DS (TA)	
Absorbance (361 nm)	Integrated Emission	Absorbance (361 nm)	Integrated Emission
0.099	1.67E+08	0.067	4.92E+07
0.076	1.42E+08	0.057	4.12E+07
0.057	1.16E+08	0.049	3.71E+07
0.029	7.23E+07	0.029	2.49E+07
0.016	3.61E+07	0.014	1.52E+07

Figure S39. Quantum Yield determination plot and data table of 8-Cl-tC^{O} DS (TT) 1X PBS Buffer at 23°C.

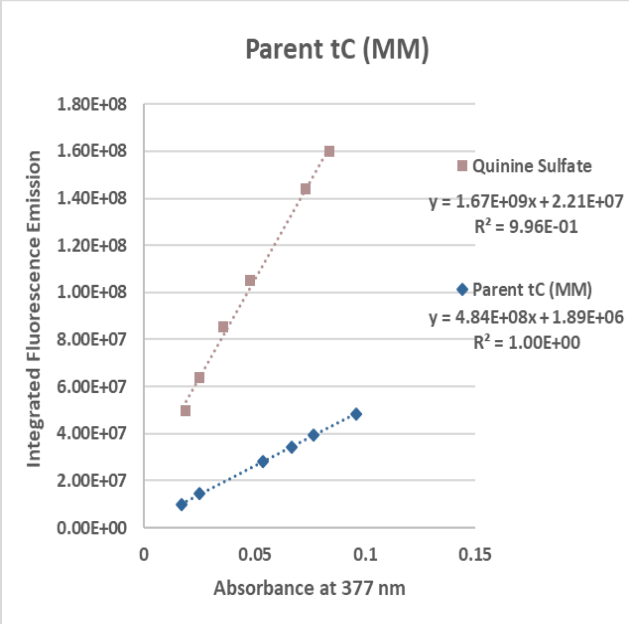

Quinine Sulfate		Parent tC (MM)	
Absorbance (377 nm)	Integrated Emission	Absorbance (377 nm)	Integrated Emission
0.084	1.60E+08	0.096	4.82E+07
0.073	1.44E+08	0.077	3.92E+07
0.048	1.05E+08	0.067	3.44E+07
0.036	8.55E+07	0.054	2.82E+07
0.025	6.36E+07	0.025	1.43E+07
0.019	4.98E+07	0.017	9.70E+06

Figure S40. Quantum Yield determination plot and data table of Parent tC (MM) in 1X PBS Buffer at 23°C.

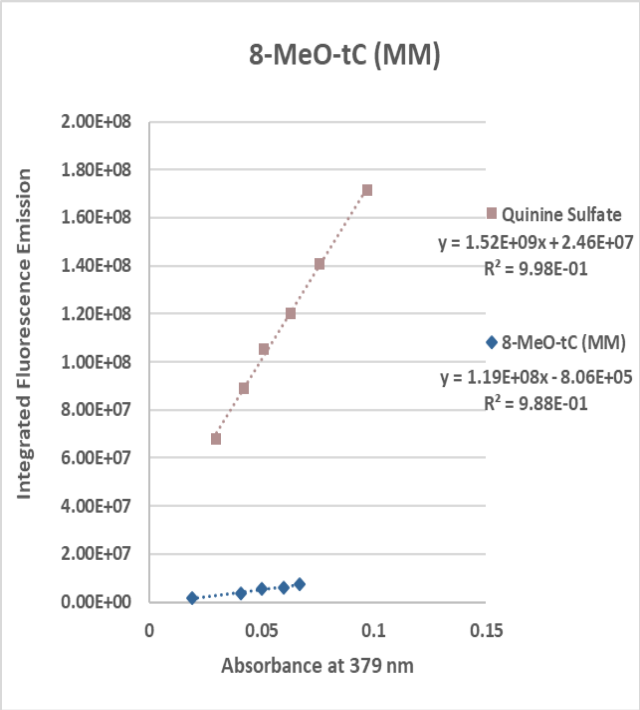

Quinine Sulfate		8-MeO-tC (MM)	
Absorbance (379 nm)	Integrated Emission	Absorbance (379 nm)	Integrated Emission
0.097	1.71E+08	0.067	7.25E+06
0.076	1.41E+08	0.060	6.26E+06
0.063	1.20E+08	0.050	5.40E+06
0.051	1.05E+08	0.041	3.69E+06
0.042	8.91E+07	0.019	1.58E+06
0.030	6.80E+07		

Figure S41. Quantum Yield determination plot and data table of 8-MeO tC (MM) 1X PBS Buffer at 23°C.

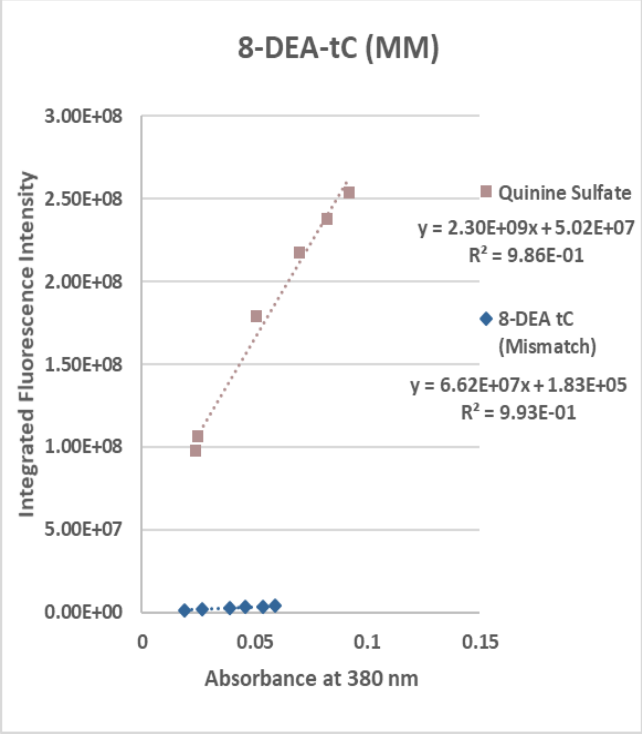

Quinine Sulfate		8-DEA-tC (MM)	
Absorbance (380 nm)	Integrated Emission	Absorbance (380 nm)	Integrated Emission
0.092	2.54E+08	0.059	4.11E+06
0.082	2.38E+08	0.054	3.62E+06
0.07	2.18E+08	0.046	3.33E+06
0.051	1.79E+08	0.039	2.85E+06
0.025	1.07E+08	0.027	1.96E+06
0.024	9.75E+07	0.029	1.39E+06

Figure S42. Quantum Yield determination plot and data table of 8-DEA-tC (MM) in 1X PBS Buffer at 23°C.

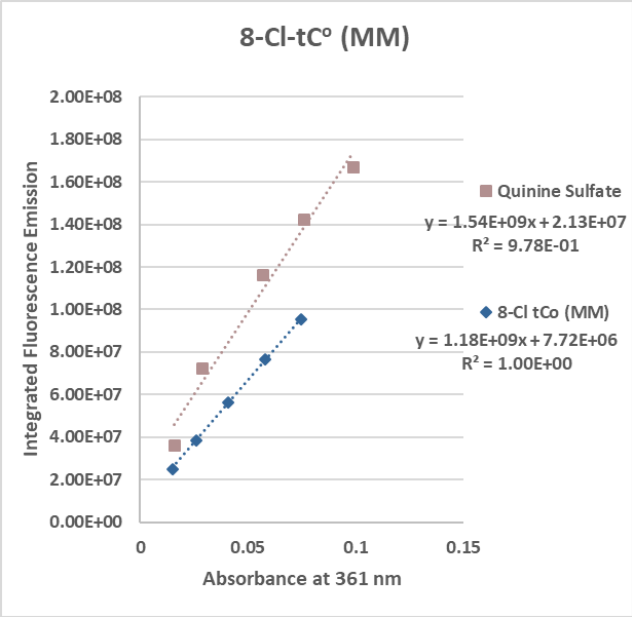

Quinine Sulfate		8-Cl-tC° (MM)	
Absorbance (361 nm)	Integrated Emission	Absorbance (361 nm)	Integrated Emission
0.099	1.67E+08	0.075	9.56E+07
0.076	1.42E+08	0.058	7.67E+07
0.057	1.16E+08	0.041	5.64E+07
0.029	7.23E+07	0.026	3.83E+07
0.016	3.61E+07	0.015	2.51E+07

Figure S43. Quantum Yield determination plot and data table of 8-Cl tC^{O} (MM) in 1X PBS Buffer at 23°C.

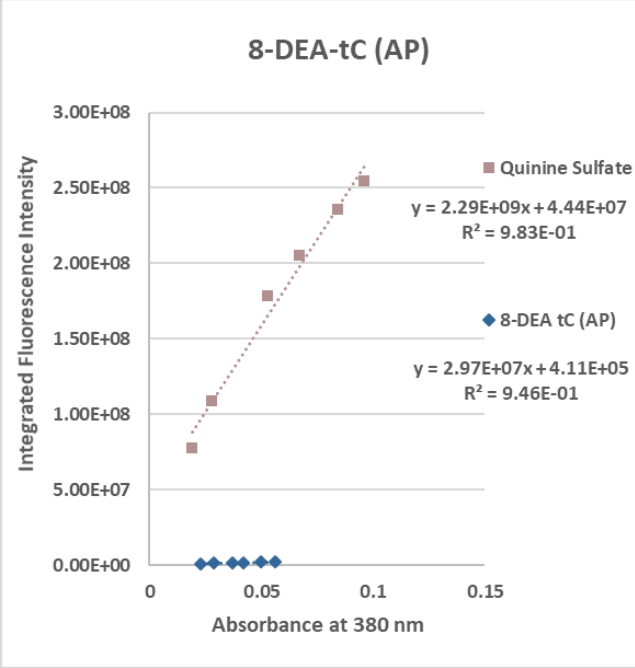

Quinine Sulfate		8-DEA-tC (AP)	
Absorbance (380 nm)	Integrated Emission	Absorbance (380 nm)	Integrated Emission
0.096	2.55E+08	0.056	1.97E+06
0.084	2.36E+08	0.050	1.95E+06
0.067	2.06E+08	0.042	1.80E+06
0.053	1.78E+08	0.037	1.48E+06
0.028	1.09E+08	0.029	1.29E+06
0.019	7.78E+07	0.023	1.03E+06
		0.021	8.56E+05

Figure S44. Quantum Yield determination plot and data table of 8-DEA tC (AP) in 1X PBS Buffer at 23°C.

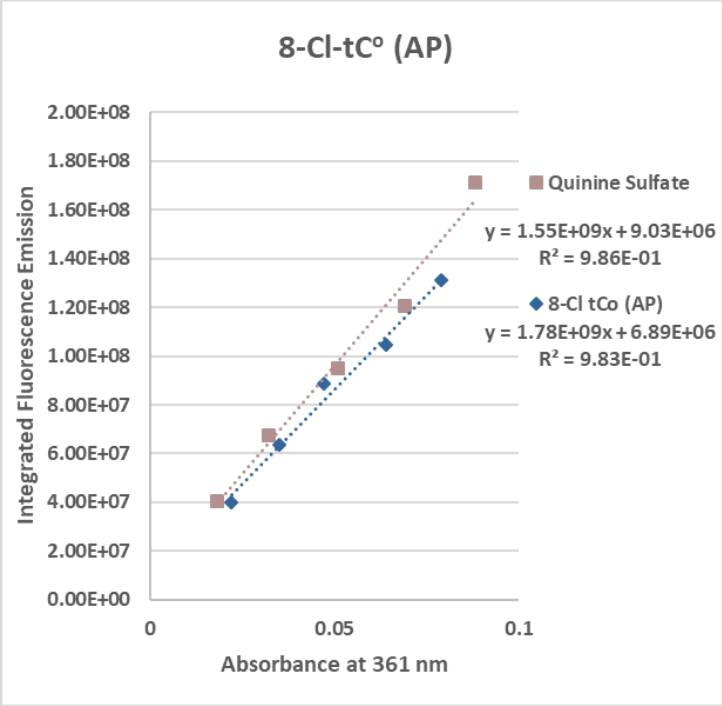

Quinine Sulfate		8-Cl-tCo (AP)	
Absorbance (361 nm)	Integrated Emission	Absorbance (361 nm)	Integrated Emission
0.088	1.71E+08	0.079	1.31E+08
0.069	1.21E+08	0.064	1.04E+08
0.051	9.48E+08	0.047	8.85E+07
0.032	6.75E+07	0.035	6.36E+07
0.018	4.04E+07	0.022	4.00E+07

Figure S45. Quantum Yield determination plot and data table of 8-Cl tC^{O} (AP) 1X PBS Buffer at 23°C.

6. Plotted absorption and emission spectra

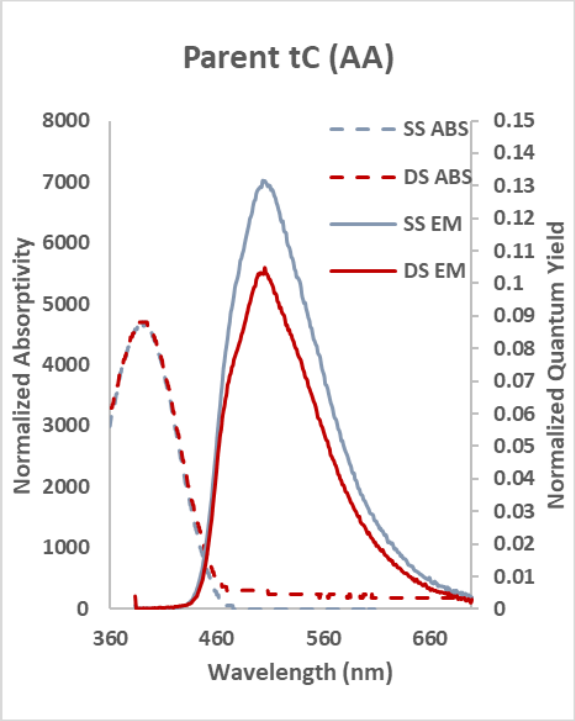

Figure S46. Absorption and emission plots of Parent tC (AA) in 1X PBS at 23°C.

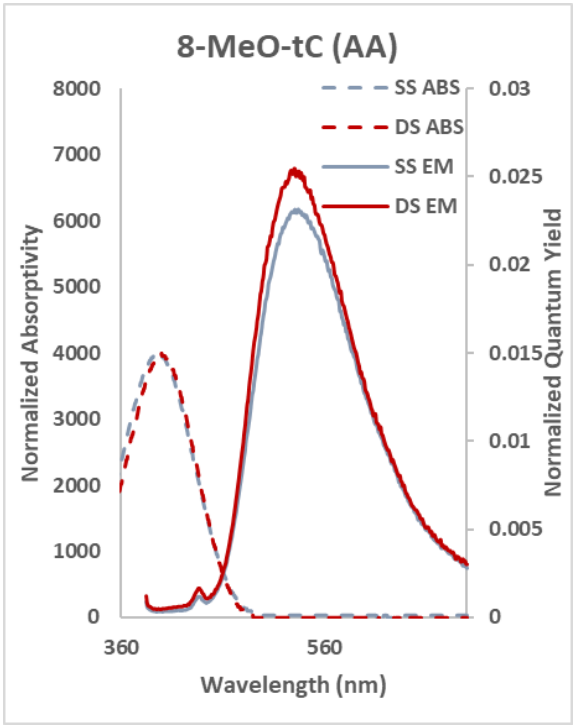

Figure S47. Absorption and emission plots of 8-MeO-tC (AA) in 1X PBS at 23°C.

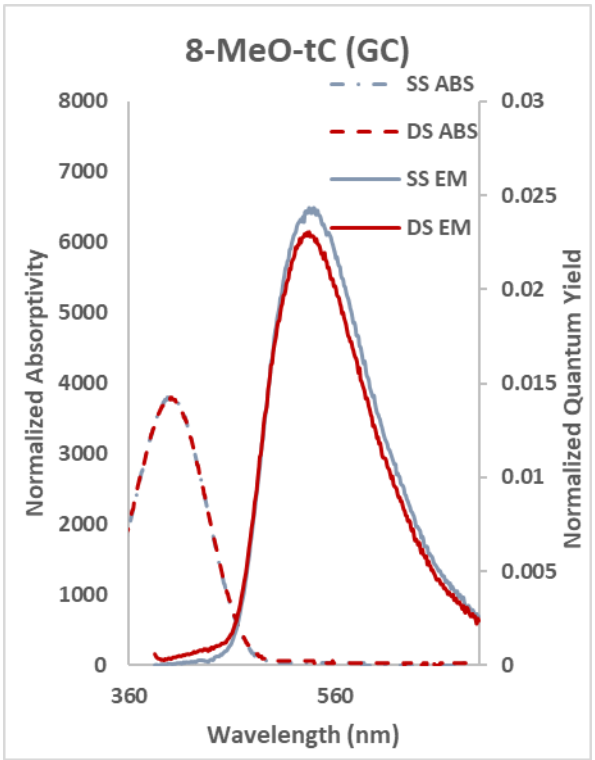

Figure S48. Absorption and emission plots of 8-MeO-tC (GC) in 1X PBS at 23°C.

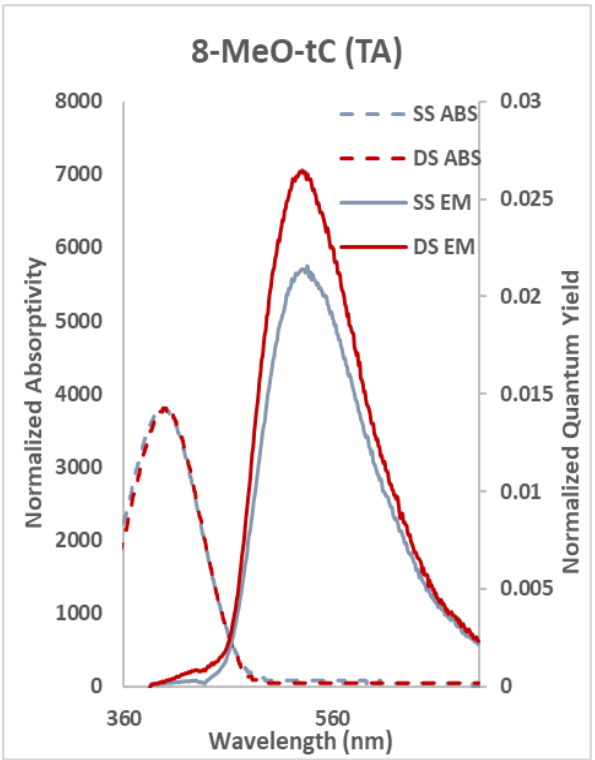

Figure S49. Absorption and emission plots of 8-MeO-tC (TA) in 1X PBS at 23°C.

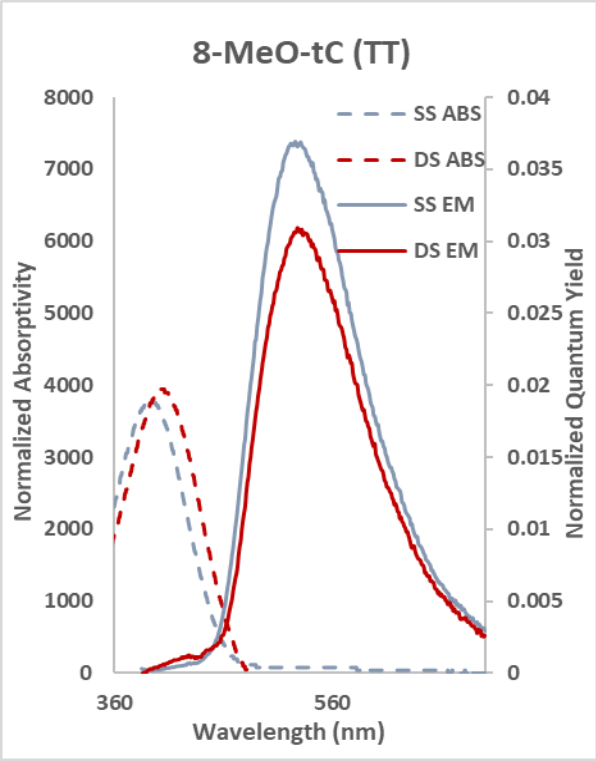

Figure S50. Absorption and emission plots of 8-MeO-tC (TT) in 1X PBS at 23°C.

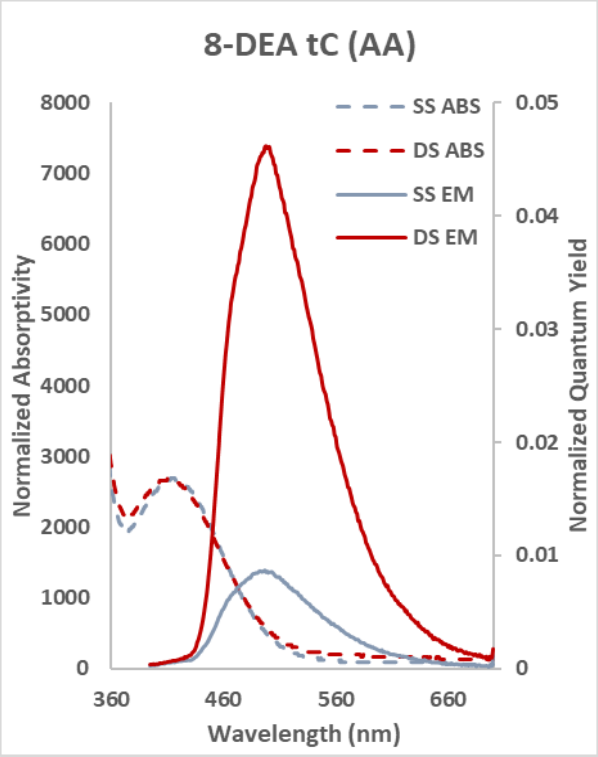

Figure S51. Absorption and emission plots of 8-DEA tC (AA) in 1X PBS at 23°C.

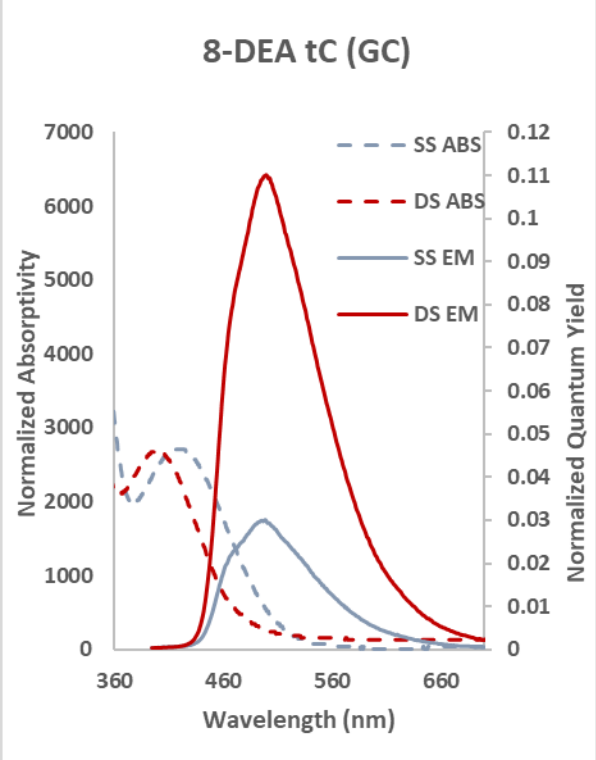

Figure S52. Absorption and emission plots of 8-DEA tC (GC) in 1X PBS at 23°C.

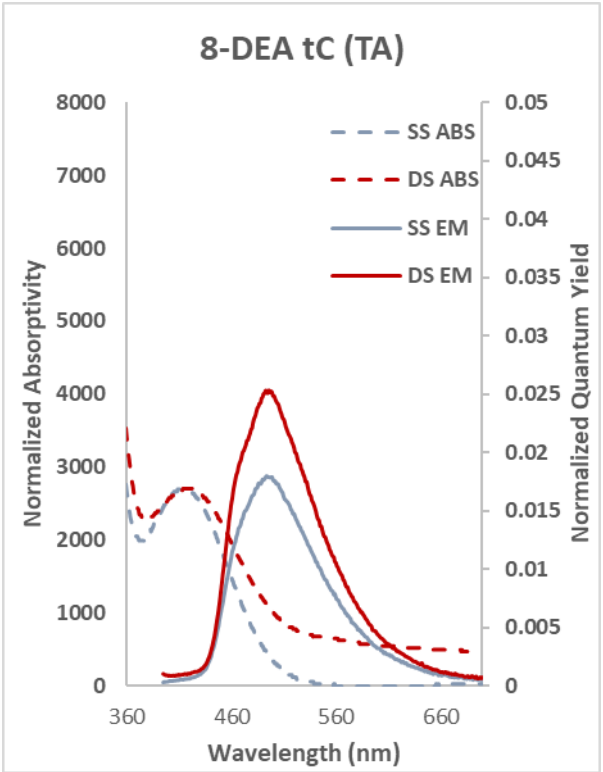

Figure S53. Absorption and emission plots of 8-DEA tC (TA) in 1X PBS at 23°C.

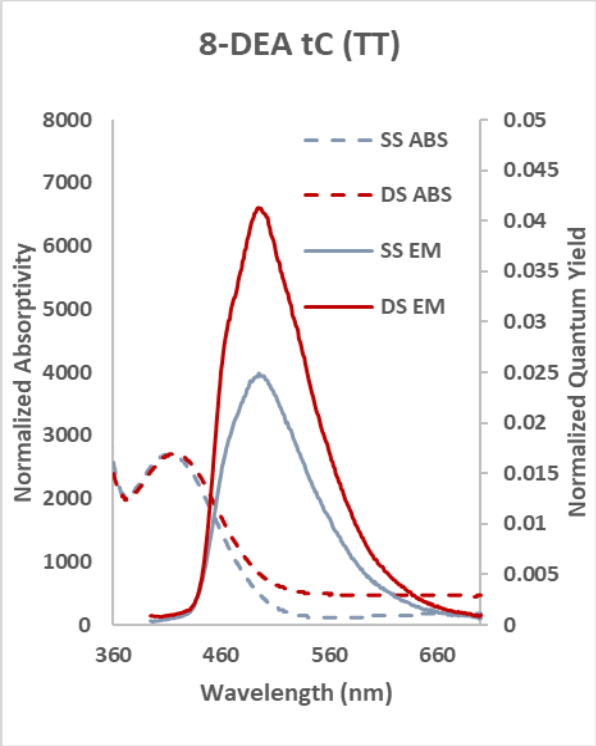

Figure S54. Absorption and emission plots of 8-DEA tC (TT) in 1X PBS at 23°C.

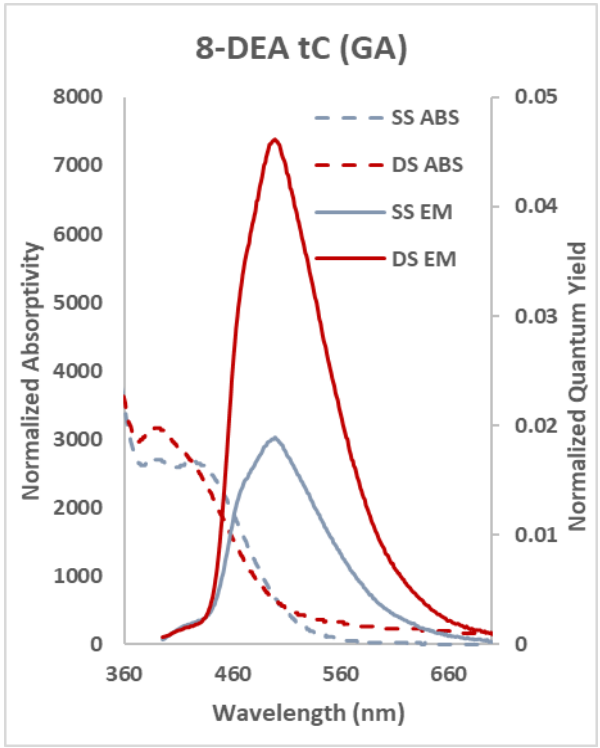

Figure S55. Absorption and emission plots of 8-DEA tC (GA) in 1X PBS at 23°C.

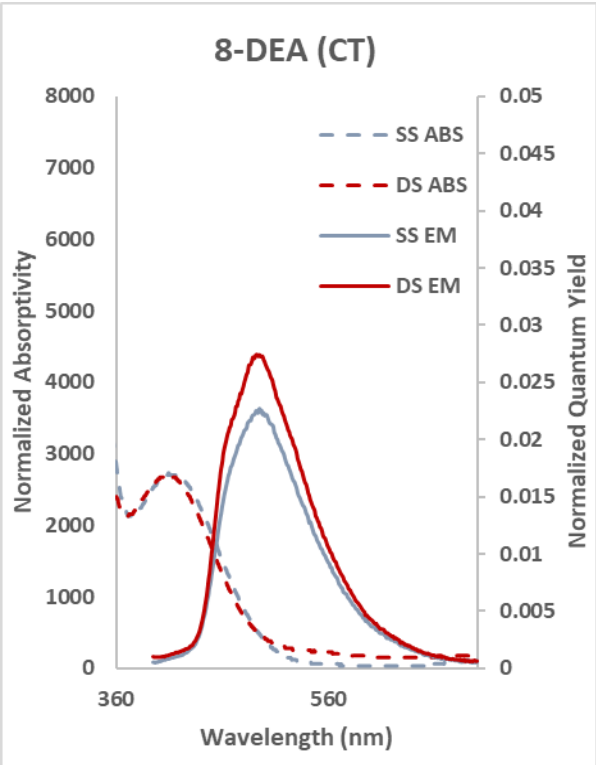

Figure S56. Absorption and emission plots of 8-DEA tC (CT) in 1X PBS at 23°C.

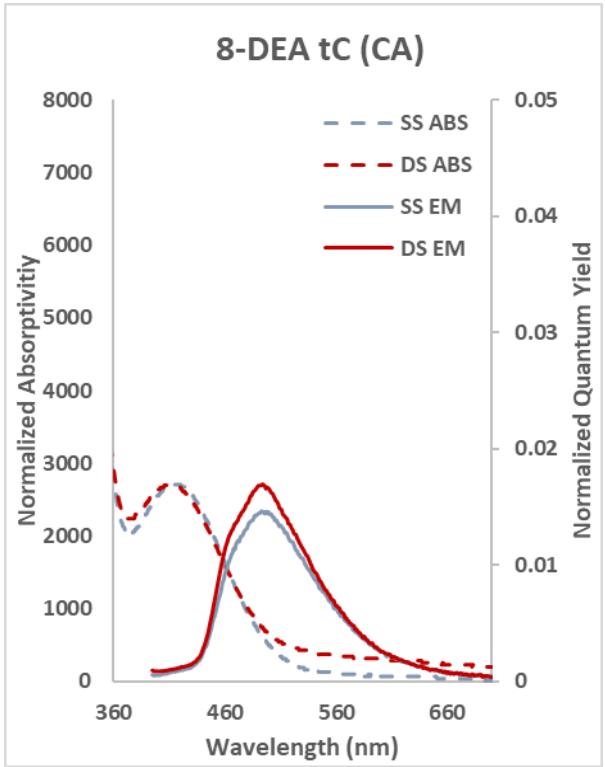

Figure S57. Absorption and emission plots of 8-DEA tC (CA) in 1X PBS at 23°C.

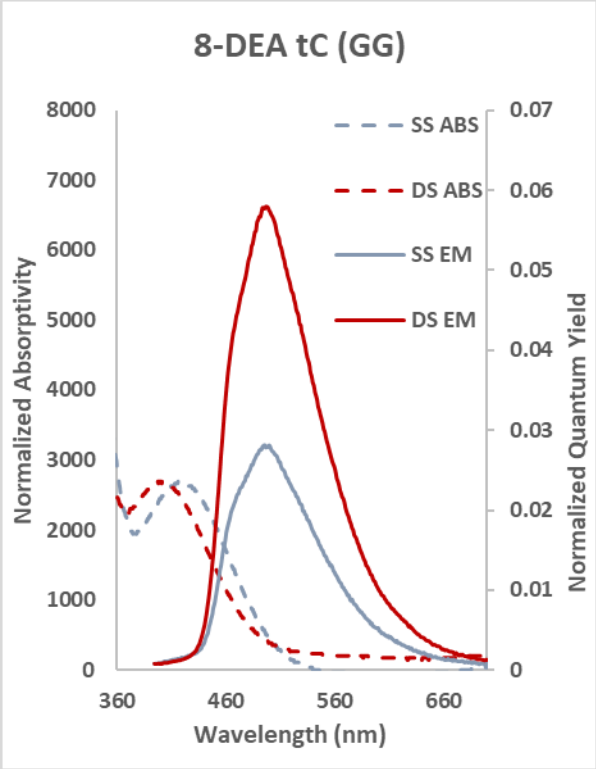

Figure S58. Absorption and emission plots of 8-DEA tC (GG) in 1X PBS at 23°C.

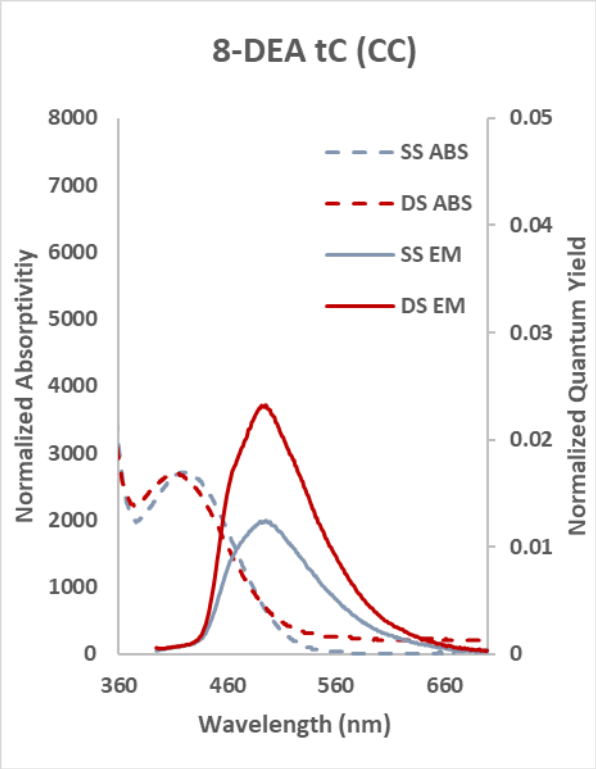

Figure S59. Absorption and emission plots of 8-DEA tC (CC) in 1X PBS at 23°C.

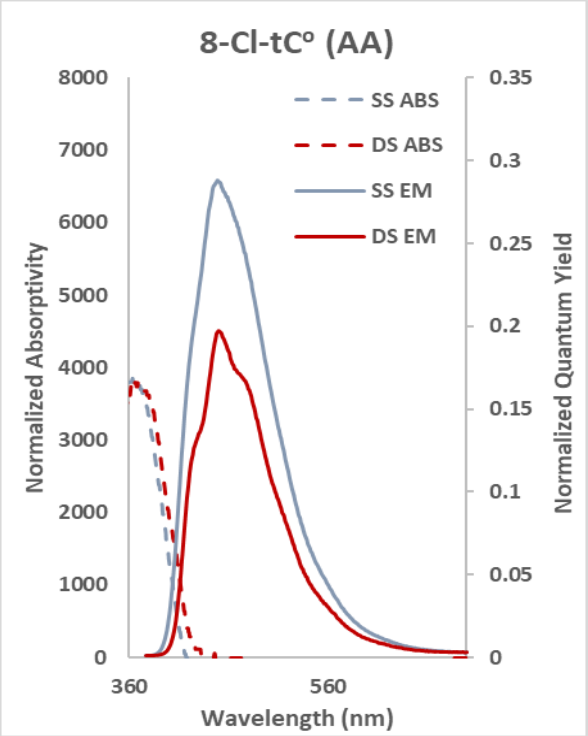

Figure S60. Absorption and emission plots of 8-Cl-tC° (AA) in 1X PBS at 23°C.

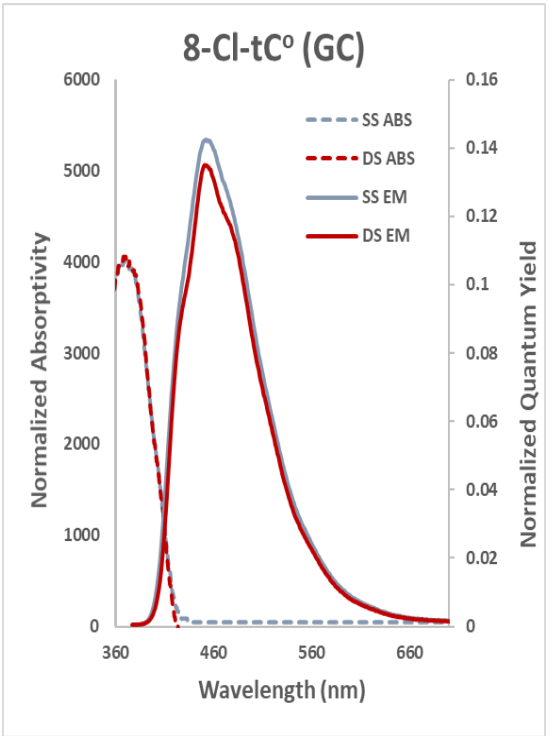

Figure S61. Absorption and emission plots of 8-Cl-tC° (GC) in 1X PBS at 23°C.

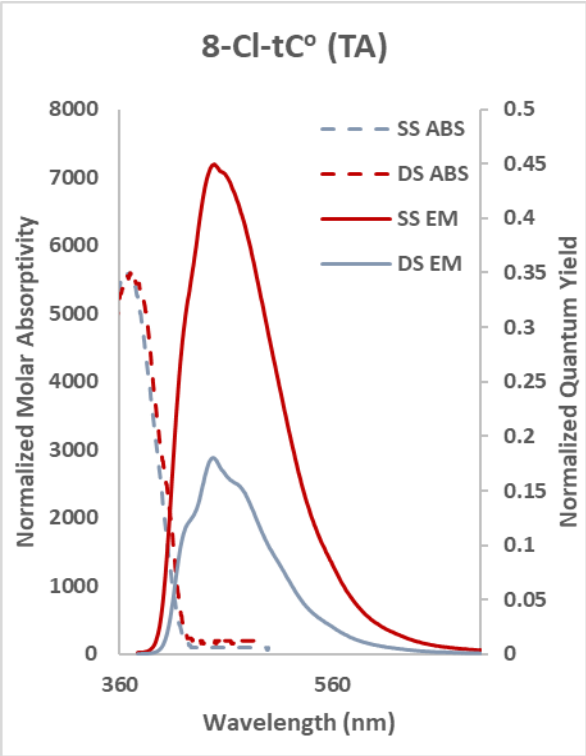

Figure S62. Absorption and emission plots of 8-Cl-tCº (TA) in 1X PBS at 23°C.

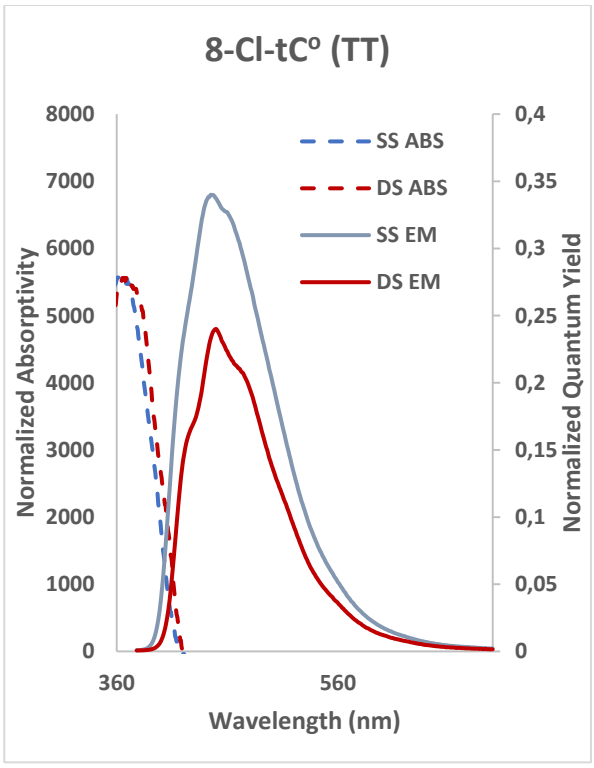

Figure S63. Absorption and emission plots of 8-Cl-tCº (TT) in 1X PBS at 23°C.

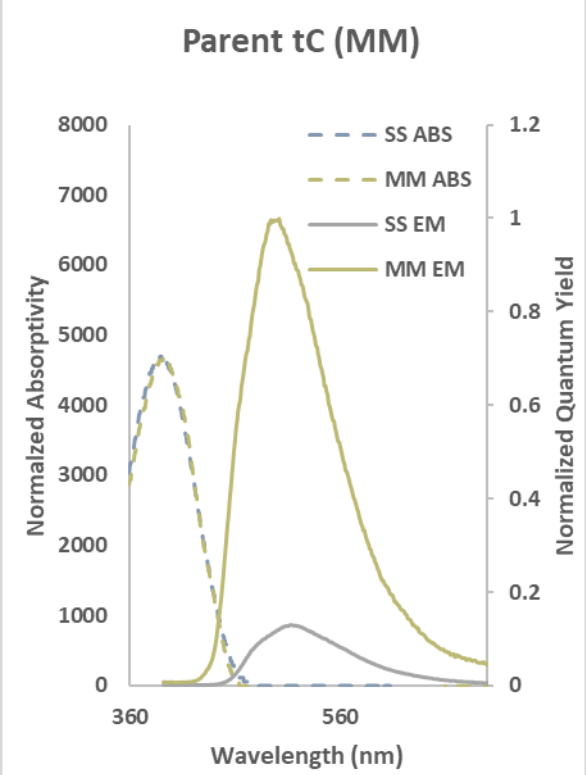

Figure S64. Absorption and emission plots of Parent tC (MM) in 1X PBS at 23°C.

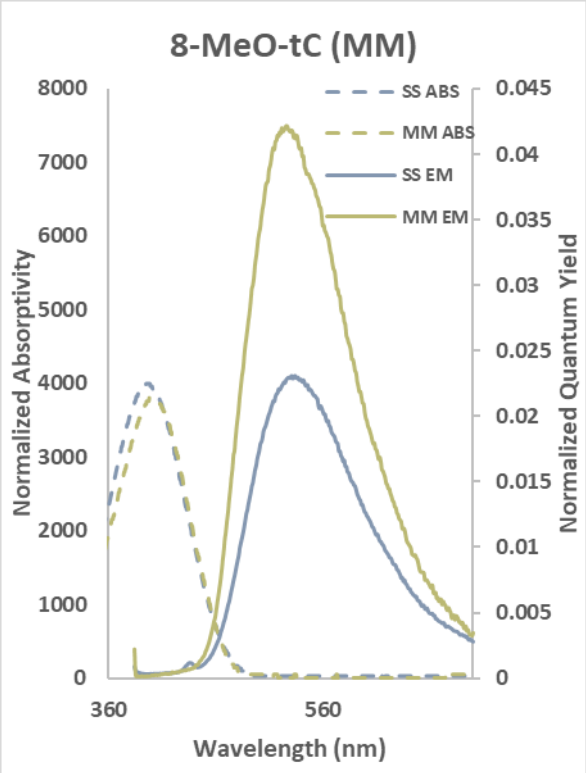

Figure S65. Absorption and emission plots of 8-MeO-tC (MM) in 1X PBS at 23°C.

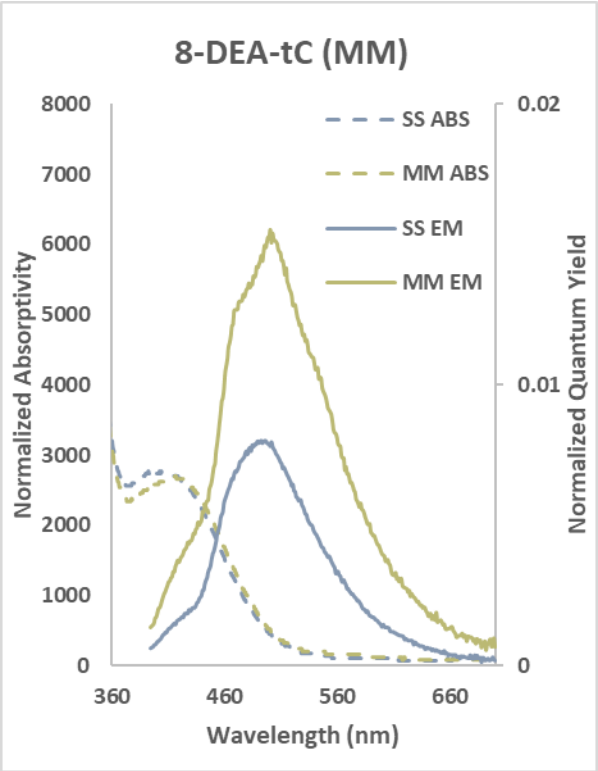

Figure S66. Absorption and emission plots of 8-DEA tC (MM) in 1X PBS at 23°C.

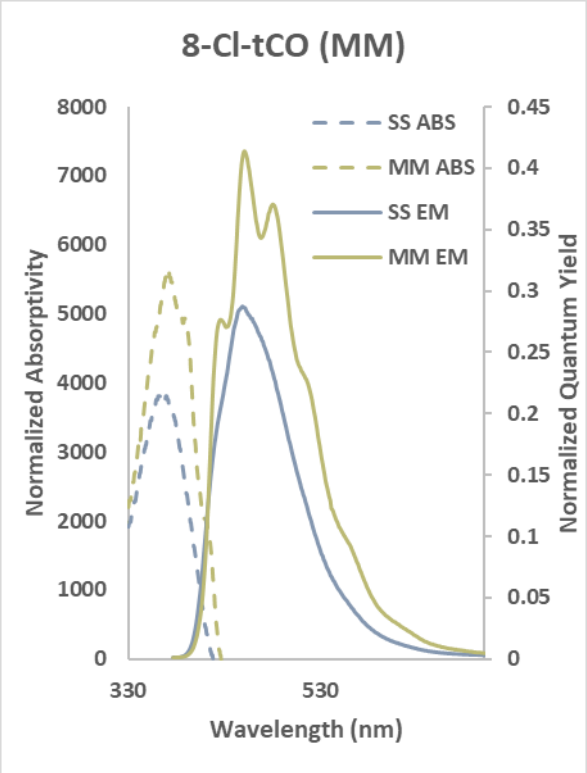

Figure S67. Absorption and emission plots of 8-Cl-tC^{o} (MM) in 1X PBS at 23°C.

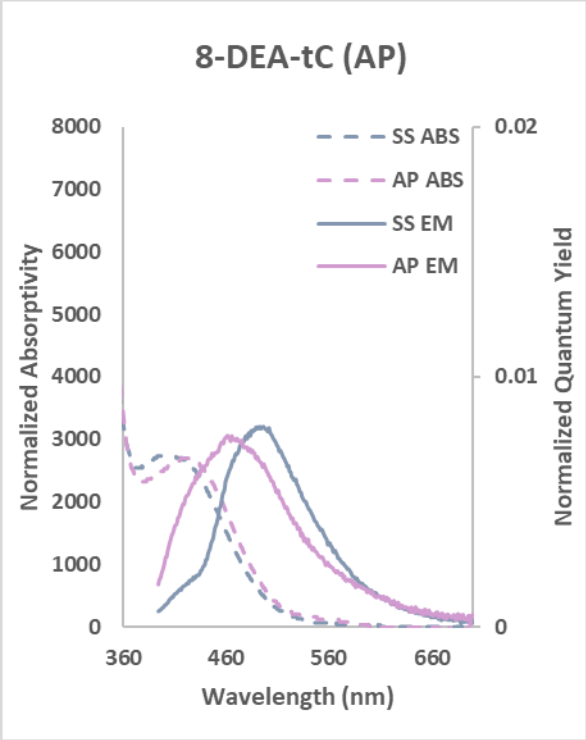

Figure S68. Absorption and emission plots of 8-DEA tC (AP) in 1X PBS at 23°C.

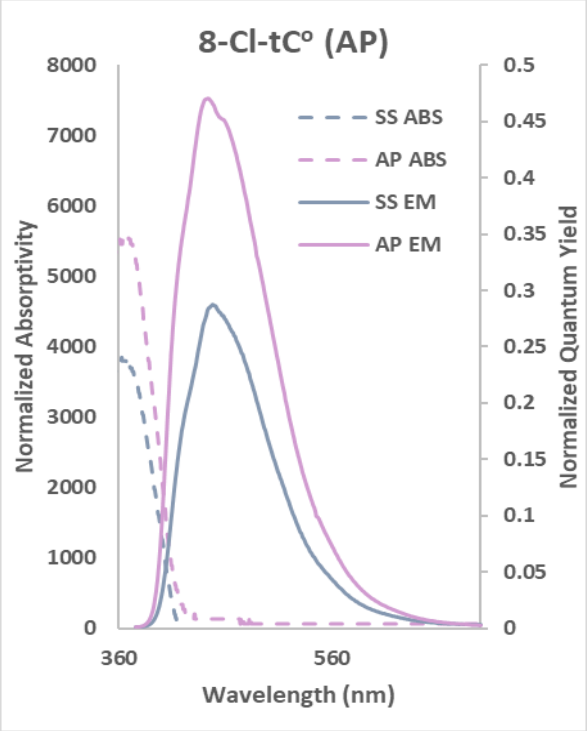

Figure S69. Absorption and emission plots of 8-Cl-tC^{o} (AP) in 1X PBS at 23°C.

7. 8-CN tC^{o} pKa Determination

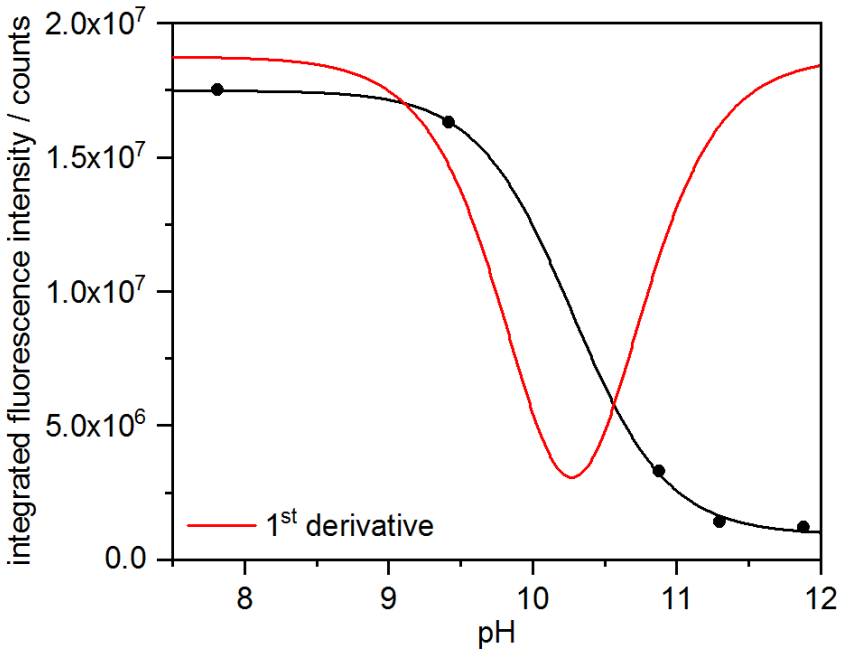

Figure S70. Fluorescence of 8-CN-tC^{O} as a function of pH.

9. Circular Dichroism Data

UV CD spectra of oligonucleotide duplexes at a concentration of 5 μM in phosphate buffered saline (10 mM sodium phosphate, pH 7.4, 27 mM potassium chloride, 137 mM sodium chloride) were collected at 25°C in a 1 cm path length cell on an Aviv model 420 spectrophotometer equipped with a Peltier temperature controller. Background-subtracted spectra were smoothed and normalized to concentration using A_{260nm} as calculated from detector voltage using the following equation and converted to standard units.

$$\text{Abs} = \log\left(\frac{\text{Voltage}_{\text{sample}}}{\text{Voltage}_{\text{solvent}}}\right) * 7.4$$

Elipticity at 255 nm was monitored from 15ºC to 75ºC at 1ºC increments. The T_M of each duplex was calculated by fitting the raw data to a two-state model in Igor Pro. Melting curves are reported as fraction unfolded.

$$\alpha_U = \frac{\theta_i - \theta_F}{\theta_U - \theta_F}$$

Where θ is ellipticity in mdeg and subscripts U and F indicate signals of strand-separated and duplex DNA, respectively.

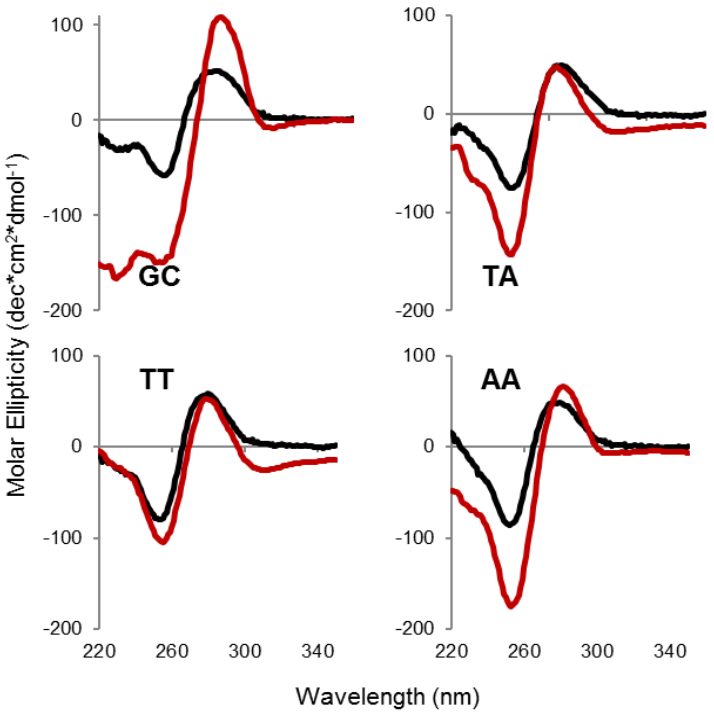

Figure S71. Circular dichroism wavelength spectra of native oligonucleotides (black) and those containing 8-Cl-tC (red).

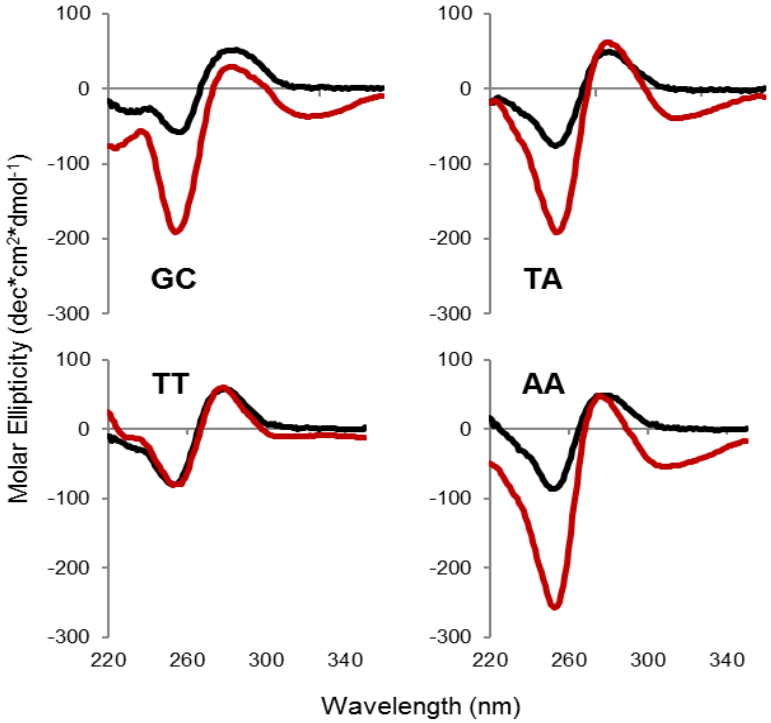

Figure S72. Circular dichroism wavelength spectra of native oligonucleotides (black) and those containing 8-MeO-tC (red).

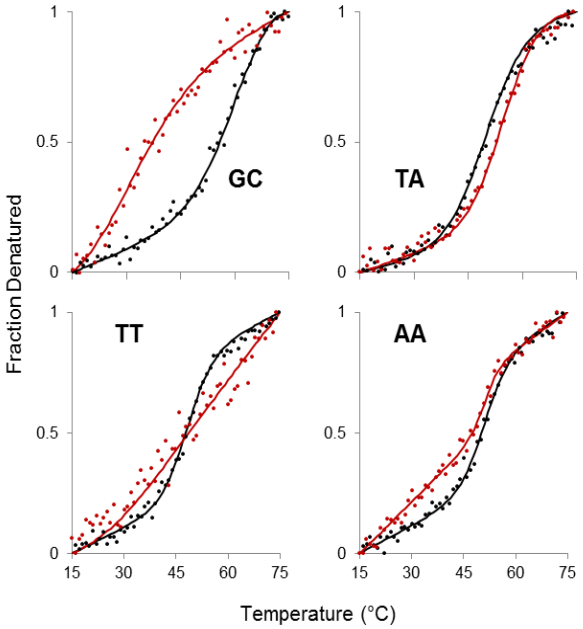

Figure S73. Duplex strand separation monitored by circular dichroism signal at 254 nm as a function of temperature. Data (markers) and two-state model fits (lines) for native oligonucleotides (black) and oligonucleotides containing 8-Cl-tC° (red), converted to fraction denatured.

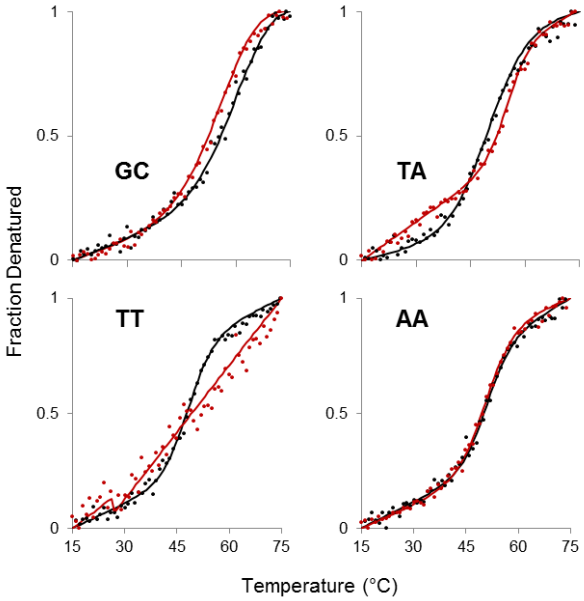

Figure S74. Duplex strand separation monitored by circular dichroism signal at 254 nm as a function of temperature. Data (markers) and two-state model fits (lines) for native oligonucleotides (black) and oligonucleotides containing 8-MeO-tC (red), converted to fraction denatured.

Denaturation temperatures calculated from circular dichroism temperature experiments

	8-MeO-tC		8-Cl-tC°	
	T_M (°C)	ΔT_M (°C)	T_M (°C)	ΔT_M (°C)
GC	59.2	-4.4	29.6	-34
TA	55.5	+5.2	55.3	+5.0
TT	non-sigmoid	N/A	non-sigmoid	N/A
AA	50.8	-0.2	51.4	+0.4

10. References

(1) Rodgers, B. J.; Elsharif, N. A.; Vashisht, N.; Mingus, M. M.; Mulvahill, M. A.; Stengel, G.; Kuchta, R. D.; Purse, B. W. *Chem. - A Eur. J.* **2014**, *20* (7), 2010–2015.

(2) Becke, A. D. *J. Chem. Phys.* **1993**, *98* (2), 1372–1377.

(3) Lee, C.; Yang, W.; Parr, R. G. *Phys. Rev. B* **1988**, *37* (2), 785–789.

(4) Becke, A. D. *Phys. Rev. A* **1988**, *38* (6), 3098–3100.

(5) Perdew, J. P.; Burke, K.; Ernzerhof, M. *Phys. Rev. Lett.* **1996**, *77* (18), 3865–3868.

(6) Zhao, Y.; Truhlar, D. G. *Theor. Chem. Acc.* **2008**, *120* (1–3), 215–241.

(7) Schäfer, A.; Horn, H.; Ahlrichs, R. *J. Chem. Phys.* **1992**, *97* (4), 2571–2577.

(8) Schäfer, A.; Huber, C.; Ahlrichs, R. *J. Chem. Phys.* **1994**, *100* (8), 5829–5835.

(9) Dunning Jr, T. H. *J. Chem. Phys.* **1989**, *90* (1989), 1007.

(10) Jensen, F. *J. Chem. Phys.* **2001**, *115* (20), 9113–9125.

(11) Tomasi, J.; Mennucci, B.; Cammi, R. *Chem. Rev.* **2005**, *105* (8), 2999–3094.

(12) Grimme, S. *J. Comput. Chem. 27* (15), 1787–1799.

(13) Frisch, M. J.; Trucks, G. W.; Schlegel, H. B.; Scuseria, G. E.; Robb, M. A.; Cheeseman, J. R.; Scalmani, G.; Barone, V.; Mennucci, B.; Petersson, G. A.; Nakatsuji, H.; Caricato, M.; Li, X.; Hratchian, H. P.; Izmaylov, A. F.; Bloino, J.; Zheng, G.; Sonnenberg, J. L.; Hada, M.; Ehara, M.; Toyota, K.; Fukuda, R.; Hasegawa, J.; Ishida, M.; Nakajima, T.; Honda, Y.; Kitao, O.; Nakai, H.; Vreven, T.; Montgomery, J. A.; Peralta, J. E.; Ogliaro, F.; Bearpark, M.; Heyd, J. J.; Brothers, E.; Kudin, K. N.; Staroverov, V. N.; Kobayashi, R.; Normand, J.; Raghavachari, K.; Rendell, A.; Burant, J. C.; Iyengar, S. S.; Tomasi, J.; Cossi, M.; Rega, N.; Millam, J. M.; Klene, M.; Knox, J. E.; Cross, J. B.; Bakken, V.; Adamo, C.; Jaramillo, J.; Gomperts, R.; Stratmann, R. E.; Yazyev, O.; Austin, A. J.; Cammi, R.; Pomelli, C.; Ochterski, J. W.; Martin, R. L.; Morokuma, K.; Zakrzewski, V. G.; Voth, G. A.; Salvador, P.; Dannenberg, J. J.; Dapprich, S.; Daniels, A. D.; Foresman, J. B.; Ortiz, J. V.; Cioslowski, J.; Fox, D. J. *Gaussian 09, Revision D.01*; Gaussian, Inc.: Wallingford CT, 2009.

(14) Schuchardt, K. L.; Didier, B. T.; Elsethagen, T.; Sun, L.; Gurumoorthi, V.; Chase, J.; Li, J.; Windus, T. L. *J. Chem. Inf. Model.* **2007**, *47* (3), 1045–1052.

(15) Williams, A. T. R.; Winfield, S. A.; Miller, J. N. *Analyst* **1983**, *108*, 1067–1071.

(16) Noé, M. S.; Ríos, A. C.; Tor, Y. *Org. Lett.* **2012**, *14* (12), 3150–3153.